Title

Tyrosine kinase inhibitors affect sweet taste and dysregulate fate selection of specific taste bud cell subtypes via KIT inhibition.

Authors

Christina M. Piarowski[1,2], Jennifer K. Scott[1,2], Courtney E. Wilson[1,2], Heber I. Lara[3], Ernesto Salcedo[1], Andrew S. Han[1,6], Elaine T. Lam[4], Peter J. Dempsey[5], Jakob von Moltke[3], Linda A. Barlow[1,2] *

* Corresponding author: Linda.barlow@cuanschutz.edu

Affiliations

[1]Department of Cell and Developmental Biology, University of Colorado Anschutz Medical Campus, Aurora Colorado.

[2] Rocky Mountain Taste and Smell Center, University of Colorado Anschutz Medical Campus, Aurora Colorado.

[3] Department of Immunology, University of Washington, Seattle Washington.

[4] Department of Medical Oncology, University of Colorado Anschutz Medical Campus, Aurora Colorado.

[5]Department of Pediatrics, Section of Developmental Biology, University of Colorado Anschutz Medical Campus, Aurora Colorado.

[6]Developing Scholars Internship Program, Graduate Program in Cell Biology, Stem Cells and Development, University of Colorado Anschutz Medical Campus.

Abstract

Taste dysfunction, or dysgeusia, is a common side effect of many cancer drugs. Dysgeusia is often reported by patients treated with anti-angiogenic tyrosine kinase inhibitors (TKIs), which inhibit receptor tyrosine kinases (RTKs). However, the mechanisms by which TKIs cause dysgeusia are not understood, as the role of RTKs in adult taste homeostasis is unknown. Here, we find that treating adult mice with the TKI cabozantinib shifts the fate of differentiating functional taste cell subtypes within taste buds. Through behavioral assays, we find this cell fate

shift leads to blunted responses to sweet in cabozantinib-treated mice. Finally, we show that inducible knockout of the RTK KIT, which is inhibited by cabozantinib, phenocopies taste cell fate shifts induced by TKI treatment. Our results establish KIT as a regulator of taste cell homeostasis and suggest that KIT inhibition may underlie TKI-induced dysgeusia in patients.

Summary

KIT signaling blockade by tyrosine kinase inhibitors alters the fate of functional taste bud cell subtypes.

Introduction

The sense of taste, or gustation, plays a central role in how animals experience the world. Taste conveys important nutritional information through five modalities: sweet, bitter, umami, sour, and salty (Liman et al., 2014). Taste dysfunction (dysgeusia) is a common side effect of many cancer therapies (Gaillard and Barlow, 2021), which leads to significantly reduced quality of life, including weight loss and depression, as well as worsened long-term outcomes for patients (Epstein and Barasch, 2010, Sánchez-Lara et al., 2010). Improving both quality of life and treatment outcomes therefore necessitates interventions that mitigate or prevent dysgeusia. However, the field lacks important mechanistic understanding of how most cancer therapies affect the taste system (Gaillard and Barlow, 2021).

One class of targeted cancer therapies that commonly cause dysgeusia are anti-angiogenic tyrosine kinase inhibitors (TKIs). These TKIs reduce tumor vascularization by inhibiting vascular endothelial growth factor receptors (VEGFRs) and platelet-derived growth factor receptor beta (PDGFRβ), both receptor tyrosine kinases (RTKs) (Vigarios et al., 2017, Kiselyov et al., 2007, Raica and Cimpean, 2010). A subset of anti-angiogenic TKIs, including cabozantinib, axitinib and sunitinib, are approved as first- and second-line therapies for metastatic renal cell carcinoma (mRCC) and cause dysgeusia in 10-50% of mRCC patients (Vigarios et al., 2017, Hahn et al., 2019, Roberto et al., 2021, Hamazaki and Uesawa, 2024). However, the intended targets, VEGFRs and PDGFRβ, are rarely found in epithelial cells, as they are expressed primarily in endothelial and stromal cells (Strell et al., 2024, Koch et al., 2011). Further, transcriptome profiling has not detected VEGFR or PDGFRβ mRNAs in murine taste epithelium (Schaum et al., 2018, Sukumaran et al., 2017, Ren et al., 2017, Yamada et al.,

2021, Golden et al., 2021, Shechtman et al., 2023, Lee et al., 2017). Cabozantinib, axitinib, and sunitinib, as well as TKIs more generally, inhibit many off-target RTKs including RET, MET, KIT, and others (Klaeger et al., 2017, Karaman et al., 2008, Davis et al., 2011). Many of these off-target RTKs are expressed in taste epithelium (Biggs et al., 2016, Choo and Dando, 2021, Donnelly et al., 2018, Mclaughlin, 2000, Sukumaran et al., 2017, Yamada et al., 2021, Wang et al., 2025), raising the possibility that inhibition of one or more off-target RTKs underlies TKI-induced dysgeusia.

Taste is mediated by taste buds, which are collections of 50-100 specialized epithelial taste bud cells (TBCs) categorized into 3 morphological types: type I, type II and type III (Delay et al., 1986, Kinnamon et al., 1993). Type I cells are glial-like support cells, type II cells detect sweet, bitter, or umami tastants, while type III cells detect sour and some salty tastants (Liman et al., 2014, Finger and Silver, 2000, Ohtubo and Yoshii, 2011, Ogata and Ohtubo, 2020). Taste buds also house specialized sodium-sensitive cells similar to type II cells in morphology, developmental regulation, and expression of many type II cell markers (Chandrashekar et al., 2010, Nomura et al., 2020, Ohmoto et al., 2020). All TBCs are short-lived, with lifespans ranging from 10 to 40 days, and are steadily generated by proliferating progenitors outside of buds (Perea-Martinez et al., 2013, Beidler and Smallman, 1965, Farbman, 1969)(and see (Barlow, 2015, Piarowski et al., 2025) for review). Despite this continual turnover, the proportions of TBC types are believed to be relatively stable throughout life (Barlow, 2015). Thus, the renewal process, spanning progenitor proliferation to TBC fate specification, differentiation, and survival, must be tightly regulated to ensure reliable taste function over time. As TKIs used to treat mRCC are frequently associated with taste dysfunction (Hamazaki and Uesawa, 2024, Vigarios et al., 2017), characterizing how these drugs impact TBC homeostasis may provide cellular and molecular mechanistic insight into how this class of TKIs causes dysgeusia.

Taste buds are housed in specialized gustatory papillae on the tongue. In rodents, fungiform papillae (FFP) are distributed throughout the anterior tongue and contain one taste bud each, while in the posterior tongue, bilateral foliate papillae and a single circumvallate papilla (CVP) at the posterior midline both comprise invaginated epithelial trenches that house hundreds of taste buds (Kinnamon, 1991). Importantly, taste buds in all papillae detect sweet, sour, bitter, etc., although bitter sensitivity is greater in the CVP and sweet sensitivity is greater in anterior

94 FFP (Shingai and Beidler, 1985, Ninomiya et al., 1993). Additionally, specialized sodium-
95 sensing type II-like cells are found only in FFP (Chandrashekar et al., 2010). How TKIs impact
96 taste buds, and whether their impact differs between taste fields, is not known.
97 Here, we investigated the effects of anti-angiogenic TKIs on taste homeostasis using
98 lingual organoids and mouse models. We show that in the CVP, cabozantinib affects renewal of
99 type II TBC subtypes by dysregulating fate selection of differentiating type II cells such that
100 production of sweet TBCs is diminished and that of bitter/umami cells is increased. Changes in
101 type II TBC composition in CVP taste buds corresponds with blunted sweet taste behavior, thus
102 linking dysregulation of type II TBC fate selection with dysgeusia. Because sweet sensitivity is
103 greater in FFP, we were surprised to find that drug treatment did not block sweet TBC
104 differentiation and instead reduced sodium-sensing type II cells in FFP. Finally, we find that the
105 off-target RTK KIT likely regulates renewal of type II TBC subtypes in both CVP and FFP, as
106 inducible *Kit* knockout in the type II TBC lineage phenocopies TKI treatment. This work
107 provides insight into the regulation of type II TBC subtype fate selection, establishes KIT
108 signaling in this process, and implicates KIT inhibition as a driver of TKI-induced dysgeusia.
109

110 **RESULTS**

111 **TKIs selectively affect sweet type II TBCs in lingual organoids.**

112 We first used lingual organoids to screen the effect of TKIs on taste bud homeostasis, as
113 organoids generated from GFP^{+} taste progenitors from the CVP epithelium of adult $Lgr5^{CreER-}$
114 ^{eGFP} mice contain all TBC types, non-taste epithelial cells and progenitors (Shechtman et al.,
115 2021, Ren et al., 2014). We assessed if three TKIs used in treatment of mRCC, cabozantinib,
116 axitinib, and sunitinib (Roberto et al., 2021, Hahn et al., 2019), hindered cell proliferation and/or
117 organoid survival during the growth phase of culture (days 2-6) (**Figure S1A**). To quantify
118 proliferation, 5-ethynyl-2'-deoxyuridine (EdU) was added to cultures for 30 minutes prior to
119 harvest; we found that TKI treatment did not alter EdU incorporation by organoids (**Figure S1B-**
120 **C**). We further assessed organoid growth by measuring organoid size at day 6. As a positive
121 control, organoids were treated with paclitaxel, which blocks cell proliferation (Weaver, 2014).
122 These organoids were significantly smaller than negative controls, whereas TKI treatment had
123 little to no impact on organoid growth. Organoids treated with 100nM axitinib were significantly
124 smaller, but this difference was small compared to the impact of paclitaxel (**Figure S2A**).

125 Results with a Cell-Titer Glo® 3D assay, which measures ATP luminescence as a proxy for cell
126 survival, were congruent with organoid size; paclitaxel decreased luminescence compared to
127 controls, whereas TKIs, including 100nM axitinib, had no impact (**Figure S2B**). Lastly, we
128 quantified organoid survival at day 6 and found 40-60% of isolated *Lgr5*-GFP$^+$ progenitors
129 formed organoids regardless of condition (**Figure S2C-D**). In sum, our data indicate that
130 cabozantinib, axitinib, and sunitinib do not affect taste progenitor proliferation or survival *in*
131 *vitro*.
132 Next, to test if TKIs affect TBC differentiation, we treated organoids during the
133 differentiation phase of culture (days 6-12) (**Figure 1A**). Organoids were harvested for
134 immunofluorescence (IF) for markers of type I (NTPDase2$^+$) (Bartel et al., 2006), type II
135 (PLCβ2$^+$) (Clapp et al., 2004), and type III (CAR4$^+$)(Chandrashekar et al., 2009) TBCs. The
136 prevalence of TBC types did not differ in TKI-treated versus control organoids (**Figures 1B-C**,
137 **S3A-D**). Type II TBCs comprise functional subsets, and those in the CVP that detect bitter or
138 umami express the G-protein GUSTDUCIN (GUST) (Kim et al., 2003). However, GUST$^+$ TBC
139 prevalence was also unaffected by TKI treatment (**Figure 1D-E**). Thus, TKIs did not impact
140 differentiation of type I, II, III, or bitter/umami type II TBCs *in vitro*.
141 To determine if TKIs affect other taste epithelial cell populations in organoids, we
142 expanded our panel of markers using RT-qPCR. Expression of *Kcnq1*, expressed by all TBCs
143 (Wang et al., 2009), and *Krt13*, a marker of non-taste CVP epithelium (Iwasaki et al., 2011), was
144 unchanged by drug treatment, suggesting that production of taste versus non-taste lineages was
145 unaffected by TKIs (**Figure S3E-F**). Consistent with immunostaining, markers of type I (*Kcnj1*)
146 (Dvoryanchikov et al., 2009), type II (*Plcβ2*), and type III (*Pkd2l1*) (Kataoka et al., 2008) TBCs,
147 as well as bitter/umami TBCs (*Gnat3* - encodes GUST) were unaffected by TKIs (**Figures 1F-G**,
148 **S3G-H**). Surprisingly, we found that markers of the sweet subset of type II TBCs were
149 specifically reduced. Expression of the G-protein coupled receptor *Tas1r2,* which
150 heterodimerizes with TAS1R3 to mediate sweet transduction (Nelson et al., 2001), was
151 decreased by all three TKIs (**Figure 1H).** *Pcdh20*, another sweet cell marker (Hirose et al.,
152 2020), was also reduced significantly by cabozantinib and expression trended downward with
153 sunitinib (p=0.07) (**Figure 1I).** These data suggest that TKIs selectively affect sweet type II
154 TBCs, but not other cell types, in lingual organoids.
155

156 **Cabozantinib changes the cellular composition of taste buds *in vivo***

157 Since sweet TBC gene expression was reduced by TKIs *in vitro*, we asked if TKI
158 treatment specifically affected sweet type II TBCs in the CVP of adult mice. Cabozantinib was
159 selected because of its long half-life (~120 hours) (Lacy et al., 2017) and because it significantly
160 reduced expression of both sweet TBC markers tested in organoids (**Figure 1**). Mice were
161 gavaged with vehicle or cabozantinib for 2 weeks (daily) or 4 weeks (5 days/week) (**Figure 2A-**
162 **B**). Cabozantinib was well-tolerated by the mice, whose weights were stable over 4 weeks
163 (**Figure S4A**). Taste buds were also grossly unaffected; taste bud number and size did not differ
164 with treatment (**Figure S4B-I**). These data suggest that cabozantinib does not affect progenitor
165 cell output or overall renewal of taste buds, consistent with data from organoids (**Figures S1-S2**).

166 To investigate cellular changes within taste buds, we first assessed the prevalence of type
167 II (PLCβ2$^+$) and type III (SNAP25$^+$) (Yang et al., 2000) TBCs in drug-treated versus control
168 mice. As expected from results in organoids, cabozantinib did not alter the number of type II or
169 III cells (**Figure 2C-H).** Consistent with reduced *Tas1r2* expression in organoids, however, drug
170 treatment significantly diminished the number of *Tas1r2*$^+$ sweet TBCs *in vivo* (**Figure 2I-K**). In
171 contrast to organoids, however, where GUST$^+$ type II TBCs were unaffected, cabozantinib
172 increased GUST$^+$ type II cells in CVP taste buds (**Figure 2L-N**). Thus, while the total number of
173 type II cells was unaffected, TKI treatment shifted type II TBC subtype composition; *Tas1r2*$^+$
174 sweet cells were reduced with a concomitant increase in GUST$^+$ bitter/umami cells. Importantly,
175 this phenotype was progressively robust with longer drug treatment (**Figure 2**), suggesting that
176 the shift in type II subtypes depends on gradual turnover of TBCs.

177 *In vivo* TKI treatment revealed an increase in GUST$^+$ bitter/umami cells not seen in
178 organoids. Upon closer inspection, we found that GUST$^+$ type II cells were over-represented in
179 CVP-derived organoids compared to their proportion in CVP taste buds (80% vs 60%,
180 respectively, of PLCβ2$^+$ type II cells are GUST$^+$) (**Figure S5A-B**). Thus, over-representation of
181 GUST$^+$ TBCs in organoids may have obscured any smaller increases in this cell population
182 caused by drug treatment.

183

184 **Cabozantinib does not shift cell type composition via cell death or transdifferentiation.**

185 As cabozantinib significantly reduced *Tas1r2*$^+$ sweet cells and increased GUST$^+$
186 bitter/umami cells in the CVP, we reasoned this shift could be due to: (1) decreased sweet TBC

187 survival, (2) transdifferentiation of sweet cells into bitter/umami cells, or (3) a shift in fate of
188 newly differentiated type II cells. A previous study revealed that the RTK KIT is expressed by
189 TAS1R3^{+} TBCs, which encompass sweet and umami type II TBC subtypes in CVP (Choo and
190 Dando, 2021). More recently, KIT has been identified as a specific marker of sweet cells (Ki et
191 al., 2025). Using hybridization chain reaction (HCR) *in situ* hybridization, we confirmed that *Kit*
192 co-localizes with *Tas1r2* in CVP taste buds (**Figure S6A**). Consistent with co-expression of
193 *Tas1r2* and *Kit*, and a decrease in *Tas1r2*$^{+}$ cells in drug-treated mice (see **Figure 2**), cabozantinib
194 significantly decreased the number of KIT^{+} TBCs per CVP taste bud profile (**Figure S6B-D**).
195 These results support previous findings that *Kit* is expressed by *Tas1r2*$^{+}$ sweet type II cells in
196 CVP taste buds.
197 To assess the fate of differentiated sweet cells following drug treatment, we induced
198 lineage tracing in *Kit*$^{CreER/+}$;*Rosa26*$^{YFP/YFP}$ mice to label existing sweet cells and then treated
199 animals with vehicle or drug for 2 weeks (**Figure 3A**). If cabozantinib decreases sweet cell
200 survival, then we would expect fewer lineage traced *Kit*-YFP^{+} cells with drug treatment.
201 However, *Kit*-YFP^{+} cell number did not differ in vehicle- versus cabozantinib-treated mice,
202 indicating no impact on sweet cell survival (**Figure 3B-C**). We next examined type II subtype
203 identity of these *Kit*-YFP^{+} cells to determine if cabozantinib caused transdifferentiation of
204 differentiated sweet cells, potentially into GUST^{+} bitter/umami cells. Consistent with HCR
205 results, in controls most *Kit*-YFP^{+} cells were PLCβ2^{+} type II cells (**Figure 3D-E**). Of these,
206 ~85% were *Tas1r2*$^{+}$ sweet cells with very few GUST^{+} bitter/umami cells (**Figure 3F-I**),
207 suggesting that *Kit* is expressed in a small subset of differentiated bitter/umami cells, and/or in
208 cells that give rise to both sweet and bitter/umami cells. Regardless, cabozantinib did not change
209 the percentage of *Kit*-YFP^{+} cells expressing *Tas1r2* or GUST (**Figure 3F-I**), demonstrating that
210 differentiated sweet cells in the CVP maintain their identity and do not transdifferentiate into
211 bitter/umami type II TBCs with drug treatment.
212
213 **Cabozantinib alters the fate of differentiating type II TBC subtypes.**
214 We next asked if TKI treatment alters the fate of differentiating TBCs. Sonic Hedgehog
215 (SHH) marks post-mitotic taste precursor cells that differentiate into each of the TBC types.
216 Precursor cells enter taste buds and express *Shh* transiently (for ~24 hrs), then differentiate into
217 TBCs within 3 days (Miura et al., 2014, Miura et al., 2006). We thus employed

218 *Shh*$^{CreER/+}$;*Rosa26*$^{tdTomato/+}$ mice to track the fate of new TBCs that differentiate during drug
219 treatment (**Figure 4A**).
220 In the CVP, the number of *Shh*-Tomato^{+} TBCs was unaffected by TKI treatment,
221 indicating cabozantinib does not impede overall differentiation of TBCs from *Shh*$^{+}$ precursor
222 cells (**Figure 4B-C**). Cabozantinib also did not affect differentiation of type II TBCs broadly, as
223 ~30% of *Shh*-Tomato^{+} cells were PLCβ2^{+} regardless of treatment (**Figures 4D-E**). Since
224 cabozantinib reduced *Tas1r2*$^{+}$ cells with a commensurate increase in GUST^{+} bitter/umami cells
225 (see **Figure 2**), we hypothesized that TKI treatment would shift the fate of newly generated type
226 II TBCs from sweet to bitter/umami fate. Consistent with this prediction, cabozantinib
227 significantly increased the percentage of newly differentiated type II cells (Shh-
228 Tomato^{+}/PLCβ2^{+}) that were GUST^{+} bitter/umami cells and significantly decreased the
229 percentage that were *Tas1r2*$^{+}$/ GUST^{-} sweet cells (**Figure 4F-I**). In sum, cabozantinib does not
230 affect differentiation of type II cells in general but rather prevents differentiation of new
231 *Tas1r2*$^{+}$/GUST^{-} sweet cells, instead biasing new type II cells toward a GUST^{+} bitter/umami fate.
232 Finally, these results explain why the impact of cabozantinib was greater with prolonged dosing
233 (see **Figure 2**), as more TBCs were replaced over time with altered proportions of newly
234 differentiated type II TBC subtypes.
235
236 **Cabozantinib impacts taste behavioral preferences of mice.**
237 Because sweet TBCs in the CVP were diminished by TKI treatment, we next asked
238 whether sweet taste function was affected. To test this, we performed two behavioral assays: (1)
239 a 48hr two-bottle taste preference test, and (2) a 30 min brief-access taste test. Mice were treated
240 with vehicle or cabozantinib and tested behaviorally during the fourth week (**Figure 5A**). Mice
241 prefer sweet, and when presented with a choice will consume/lick more sweet solution than
242 water when sweet is detected above threshold (Reed and Knaapila, 2010). In two-bottle tests,
243 neither vehicle- nor cabozantinib-treated mice preferred sweet solution at low concentrations of
244 the non-nutritive sweetener SC45647 (Nofre et al., 1990). However, control mice strongly
245 preferred 100 μM SC45647, while TKI-treated mice had no preference for sweet and drank equal
246 volumes of sweetener and water (**Figure 5B**). Importantly, the total volume of solution
247 consumed was not altered by drug treatment, although control mice drank significantly more 100
248 μM SC45647, likely driven by strong preference for the sweet solution (**Figure S7A**).

249 A brief-access test with Davis Rig lickometers (Smith, 2001) was also used to assess taste
250 behavior. This apparatus allows rapid testing of multiple concentrations of tastant in a 30-minute
251 period. Moreover, limited access tests avoid post-ingestive effects that can influence taste
252 behavior (Gaillard and Stratford, 2016). As with two-bottle testing, cabozantinib did not alter
253 important metrics of drinking behavior (**Figure S7B-G**). Similarly, control mice in lickometer
254 assays strongly preferred SC45647, while TKI-treated mice showed no preference for the non-
255 nutritive sweetener (**Figure 5C**). Both two-bottle and lickometer tests reveal that cabozantinib
256 decreases behavioral preference for sweet, consistent with the histological finding of reduced
257 sweet TBCs in CVP taste buds.
258 Since cabozantinib increased bitter/umami type II cells, we also tested whether TKI
259 treatment impacted bitter taste function. As bitter is aversive to mice, we hypothesized that the
260 drug-induced increase in GUST$^+$ cells would lower the threshold for avoidance of bitter solution.
261 However, both vehicle- and cabozantinib-treated mice had comparable behavioral avoidance of
262 quinine (**Figure 5D**). We also tested sour taste, which is mediated in part by type III TBCs
263 (Liman et al., 2014). Avoidance of citric acid was not affected by drug treatment, consistent with
264 our finding that cabozantinib did not impact type III cells (**Figure 5E**). Thus, cabozantinib did
265 not affect taste preference for either bitter or sour but selectively blunted behavioral responses to
266 sweet.
267
268 **In anterior FFP, cabozantinib does not affect production of sweet TBCs but instead**
269 **reduces sodium-sensing TBCs.**
270 Although all taste qualities, including sweet, are detected by FFP and CVP taste buds, the
271 FFP taste field is more sensitive to sweet tastants and thus we predicted that sweet type II TBCs
272 in FFP would also be diminished by TKI treatment. In FFP, PLCβ2$^+$ TBCs comprise 4 functional
273 subtypes: sweet-, bitter-, umami-, and sodium-sensing. Unlike in the CVP, where *Tas1r2* and
274 GUST are largely expressed by separate PLCβ2$^+$ cell populations (sweet versus bitter/umami,
275 respectively), almost all *Tas1r2*$^+$ sweet cells in FFP co-express GUST, as do most bitter and
276 umami type II cells (Kim et al., 2003, Tomonari et al., 2011). In contrast, specialized sodium-
277 sensing TBCs express PLCβ2 and have strong developmental, molecular and morphological
278 similarities with type II cells, but lack GUST expression (Ohmoto et al., 2020, Chandrashekar et
279 al., 2010). Here, we considered all 4 functional TBC types as type II subtypes. We thus assessed

280 if type II TBC subtype proportions were altered in FFP after 4 weeks of TKI dosing, and
281 specifically if *Tas1r2*$^{+}$/GUST^{+} sweet TBCs were reduced. Unexpectedly in FFP, neither
282 *Tas1r2*$^{+}$/GUST^{+} sweet cells nor GUST^{+} bitter/umami cells were impacted by drug treatment
283 (**Figure S8I-J**). Instead, cabozantinib treatment resulted in fewer PLCβ2^{+}/GUST^{-} sodium-
284 sensing cells (**Figure S8E-H**).
285 We also assessed whether cabozantinib induced cell death or transdifferentiation of type
286 II TBCs in FFP (see **Figure 3**). As in the CVP, cabozantinib had no impact on TBC survival as
287 the number of *Kit*-YFP^{+} cells was unchanged (**Figure S9A-B**). Interestingly, while *Kit*-YFP
288 primarily labels sweet type II cells in the CVP, *Kit*-YFP lineage traced into all three type II TBC
289 subtypes at similar proportions in FFP; ~60% of YFP^{+} cells were GUST^{+} (30% were Tas1r2^{+}
290 sweet cells, meaning the other ~30% were likely bitter/umami cells) and ~40% were GUST^{-}
291 sodium-sensing cells (**Figure S9C-H**). Regardless, cabozantinib did not change the percentage
292 of *Kit*-YFP^{+} cells expressing PLCβ2, GUST or *Tas1r2* and thus did not induce
293 transdifferentiation in FFP taste buds (**Figure S9C-H**).
294 Finally, we assessed the fate of TBCs newly differentiated from *Shh*$^{+}$ precursor cells in
295 FFP taste buds (see **Figure 4A**). As in the CVP, drug treatment did not affect differentiation of
296 *Shh*-Tomato^{+} cells nor the percentage of *Shh*-Tomato^{+} cells differentiating as PLCβ2^{+} type II
297 TBCs (**Figure S10A-D**). Instead, cabozantinib significantly increased the percentage of *Shh*-
298 Tomato^{+}/PLCβ2^{+} cells that were GUST^{+} and decreased the percentage that were GUST^{-}
299 (sodium-sensing) (**Figure S10E-F**). Since differentiation of *Tas1r2*$^{+}$/GUST^{+} sweet cells was
300 unchanged (**Figure S10G-H**), the increase in *Shh*-Tomato^{+}/GUST^{+} TBCs likely reflects an
301 increase in differentiated bitter/umami type II cells at the expense of GUST^{-} sodium-sensing
302 TBCs. Thus, cabozantinib alters the fate of newly generated type II TBCs, albeit different
303 subtypes, in both CVP and FFP taste buds.
304
305 **Conditional deletion of *Kit* phenocopies TKI treatment in both CVP and FFP taste buds.**
306 Three lines of evidence suggested that TKI inhibition of the off-target RTK KIT may
307 underlie shifts in type II TBC differentiation. In addition to intended targets VEGFRs and
308 PDGFRβ, KIT is inhibited by all three TKIs tested here (Klaeger et al., 2017, Karaman et al.,
309 2008, Davis et al., 2011). Further, mice treated with cabozantinib developed fur depigmentation
310 (**Figure S11**), a physiological readout of KIT inhibition in mice and humans (Moss et al., 2003).

311 Finally, *Kit* is expressed in differentiated sweet type II cells in the CVP and lineage traces into all
312 type II cell subtypes in both taste fields, suggesting the type II cell lineage may be directly
313 sensitive to KIT inhibition (see **Figures 3, S6, S9**). The POU2F3 transcription factor is expressed
314 in all type II cells and is required for their differentiation (Matsumoto et al., 2011). Thus, we
315 combined the *Pou2F3*^{CreER} allele (Mcginty et al., 2020) with a novel floxed *Kit* allele (*Kit10*)
316 wherein LoxP sites flank exon 10 that encodes the transmembrane domain of KIT protein (Lara
317 et al. 2025, in revision). To delete *Kit* in the type II TBC lineage, *Pou2F3*$^{CreER/+}$*;Kit*$^{fl/fl}$ mice
318 were dosed with tamoxifen or corn oil every other day for 2 weeks (**Figure S12A**).

319 Cre induction abolished KIT expression in CVP epithelium, indicating efficient excision
320 of *Kit* (**Figure S12B-C**). *Kit* deletion did not affect numbers of type II or type III cells (**Figure**
321 **S12D-G**), but as with drug treatment, significantly fewer *Tas1r2*$^{+}$ sweet cells were detected
322 (**Figure S12H-I**). Two weeks after *Kit* deletion, however, GUST^{+} cell number was unchanged
323 (**Figure S12J-K**). We next tested if longer term *Kit* knockout would fully recapitulate the fate
324 shift in type II TBC subtypes observed after 4 weeks of drug (see **Figure 2**). *Pou2F3*$^{CreER/+}$*;Kit*$^{fl/fl}$
325 mice were fed tamoxifen chow for 4 weeks (**Figure 6A**). As tamoxifen chow can cause weight
326 loss and other side effects (Halpage et al., 2024), control *Kit*$^{fl/fl}$ mice lacking *Pou2F3*^{CreER} were
327 also fed tamoxifen chow. Under this protocol, KIT expression was efficiently ablated in CVP
328 epithelium (**Figure 6B-C**). Consistent with 4 weeks of cabozantinib treatment, the number of
329 type II and type III cells did not significantly change with prolonged *Kit* KO (**Figure 6D-G**),
330 while *Tas1r2*$^{+}$ sweet cells were significantly decreased (**Figure 6H-I**) with a commensurate, and
331 significant, increase in GUST^{+} bitter/umami type II cells (**Figure 6J-K**). Thus, both cabozantinib
332 and *Kit* KO induce a shift in type II TBC subtype fate after 4 weeks (**Figure 6L**).

333 In FFP taste buds, POU2F3 is expressed by all PLCβ2^{+} cells, including sweet, bitter, and
334 umami type II cells, as well as by PLCβ2^{+} sodium-sensing taste cells (Ohmoto et al., 2020). As
335 in CVP, *Kit* KO in *Pou2F3*$^{+}$ cells efficiently ablated *Kit* in FFP taste buds after two weeks of
336 tamoxifen gavage (**Figure S13A-B**). As with drug treatment, conditional deletion of *Kit* did not
337 affect the number of type II or type III cells (**Figure S13C-D, G-H**), nor were *Tas1r2*$^{+}$ sweet
338 cells affected (**Figure S13E-F**). Rather, consistent with the fate shift induced by cabozantinib in
339 FFP, GUST^{-} sodium cells were decreased and GUST^{+} bitter/umami cells were increased by *Kit*
340 deletion (**Figure S13I-L**). Thus, inducible *Kit* knockout phenocopies the effects of cabozantinib

341 treatment in both FFP (**Figure S13M**) and CVP, suggesting TKIs disrupt type II TBC fate
342 selection through KIT inhibition.
343
344 **Discussion**
345 Many cancer drugs have the unintended side effect of perturbing taste. Since turnover of
346 TBCs relies upon proliferating progenitors, therapies targeting proliferating cells are especially
347 harmful to the taste system. For example, targeted head and neck irradiation, as well as anti-
348 mitotic chemotherapies, are cytotoxic to taste progenitors and disrupt TBC renewal (Jewkes et
349 al., 2018, Gaillard et al., 2019, Mukherjee et al., 2017, Ren et al., 2023). However, we find that
350 the three anti-angiogenic TKIs tested here do not affect progenitor proliferation or survival when
351 tested in lingual organoid cultures. TBC renewal can also be grossly disrupted by drugs that
352 inhibit taste cell specification. Targeted drugs that inhibit SHH signaling, which is required for
353 specification of new TBCs, prevent the specification of new taste cells and thus lead to
354 progressive taste bud degeneration as older cells are lost and not replaced (Castillo et al., 2014,
355 Castillo-Azofeifa et al., 2017, Liu et al., 2013, Kumari et al., 2015, Kumari et al., 2018, Yang et
356 al., 2015, Lu et al., 2018). TKI treatment, however, did not cause large-scale disruption of TBC
357 specification *in vivo* or *in vitro*. Instead, we find that differentiation of type II TBC subtypes
358 specifically was dysregulated by anti-angiogenic drugs. In the CVP, cabozantinib decreased
359 sweet type II cells and increased bitter/umami type II cells, while in FFP, sweet cells were not
360 affected. Instead, cabozantinib led to reduced sodium cells with a commensurate increase in
361 bitter/umami cells. Although multiple type II subtypes were altered by drug treatment,
362 surprisingly only sweet taste behavior was impacted. In the CVP and FFP, these shifts in cell fate
363 were recapitulated by deletion of *Kit* in the type II TBC lineage, suggesting that the impact of
364 TKIs on type II TBC fate is due to KIT inhibition.
365
366 **Lineage dynamics of taste renewal**
367 *Shh*$^+$ taste precursor cells differentiate into all TBC types (Miura et al., 2014). However,
368 it is not known whether these cells differentiate directly into TBCs or if further intermediate cell
369 states exist wherein additional lineage decisions are made. *Ascl1* is expressed in type III TBCs
370 and a subset of *Shh*$^+$ precursors and is required for type III cell production (Seta et al., 2006, Seta
371 et al., 2011). Lineage tracing of *Ascl1*$^+$ cells primarily labels type III cells and a small number of

372 type II cells (Matsuyama et al., 2023, Hsu et al., 2021), suggesting *Shh*$^+$ precursors co-expressing
373 *Ascl1* are capable of producing both cell types but are biased toward type III fate. In contrast,
374 *Pou2F3* is expressed by some precursor cells and all mature type II TBCs and is necessary for
375 type II cell production; *Pou2F3* knockout mice lose type II cells with a corresponding increase in
376 type III cells (Matsumoto et al., 2011). Altogether, these studies suggest a model where *Shh*$^+$
377 precursor cells become progressively lineage restricted to type III and type II cell fate by *Ascl1*
378 and *Pou2F3*, respectively. However, where in the taste lineage cells acquire type II TBC subtype
379 fates is unknown. Since knocking out *Kit* in *Pou2f3*$^+$ cells, as well as cabozantinib treatment, had
380 no effect on differentiation of type II cells broadly but rather shifted the fate of type II TBC
381 subtypes, we propose that *Shh*$^+$ descendent cells acquire type II subtype fate in POU2F3$^+$
382 lineage-restricted type II cell precursors. Since FFP sodium cells also depend on POU2F3 for
383 differentiation (Ohmoto et al., 2020), and since cabozantinib and *Kit* knockout affected the
384 differentiation of sodium cells, our data support published findings that sodium cells and type II
385 cells also arise from a common POU2F3$^+$ precursor population in FFP taste buds (Ohmoto et al.,
386 2020).

387 In both CVP and FFP, we find that *Kit* lineage tracing labels all type II TBC subtypes,
388 albeit to different degrees, whereas KIT is not expressed in all differentiated type II cells (Choo
389 and Dando, 2021, Ki et al., 2025). Together these findings suggest that KIT is expressed in
390 POU2F3$^+$ type II precursor cells. Additionally, conditional *Kit* knockout in *Pou2F3*$^+$ cells
391 revealed that KIT is required for production of the correct proportions of type II TBC subtypes.
392 Thus, we hypothesize that KIT signaling governs fate selection of differentiating type II TBCs.
393 Interestingly, a recent report found that the KIT inhibitor imatinib had no effect on normal taste
394 homeostasis (Ki et al., 2025). It is important to note that imatinib has a much shorter half-life
395 than cabozantinib (~20 hours versus ~120 hours, respectively) (Peng et al., 2005, Lacy et al.,
396 2017), and mice were treated daily for only 12 days. Since KIT inhibition likely affects type II
397 cells as they gradually turnover, and since sweet cell reduction was observed after 14 days of
398 either cabozantinib treatment or inducible *Kit* knockout, imatinib may not have been present at
399 high enough levels and/or for long enough for the effects on type II cell differentiation to become
400 apparent.

401 KIT function is required for differentiation of multiple cell types in other systems,
402 including T-cells (Krishnamoorthy et al., 2008), cardiomyocytes (Li et al., 2008), spermatogonia

403 (Nasimi et al., 2021), and melanocytes (Liao et al., 2017). Importantly, a complementary paper
404 using *Pou2F3*$^{CreER/+}$;*Kit*$^{fl/fl}$ mice identified KIT as a regulator of intestinal tuft cell hyperplasia
405 following helminth infection (Lara et al. 2025, in revision). In this context, KIT is required for
406 the proliferation and/or differentiation of tuft cells during a type II immune response. Tuft cells,
407 like type II TBCs, require POU2F3 for their generation (Gerbe et al., 2016), suggesting a shared
408 requirement of KIT signaling in regulating the differentiation of POU2F3-dependent cells in
409 multiple epithelial systems.
410
411 **Mechanisms of behavioral taste alterations**
412 In rodents, it is well established that FFP taste buds in the anterior tongue are more highly
413 tuned to sweet than posterior CVP taste buds, while posterior taste buds are more sensitive to
414 bitter (Ninomiya et al., 1993, Shingai and Beidler, 1985). Thus, we were surprised when
415 cabozantinib had no impact on sweet cell differentiation in FFP despite causing a loss of
416 behavioral preference for sweet. Instead, sweet cell loss was evident only in CVP taste buds.
417 These discordant changes in different taste papillae may contribute to TKI-induced dysgeusia, as
418 incongruent input from anterior and posterior taste fields may change how taste stimuli are
419 perceived (as proposed by (Gaillard et al., 2017)). Sweet taste behavioral responses may
420 therefore depend on balanced sweet cell renewal in FFP and CVP, as normal sweet cell number
421 in FFP did not appear to compensate for reduced sweet TBCs in the CVP. Additionally, it has
422 been proposed that FFP taste buds mediate fine taste discrimination while CVP taste buds
423 regulate a binary accept/reject response once substances reach the posterior oral cavity (Tomchik
424 et al., 2007, Travers et al., 1987, St. John and Spector, 1998). Sweet cells in the CVP could be
425 important to signal tastant acceptance, which may be required to drive appetitive behavior. Thus,
426 a reduction in CVP sweet cells may lower tastant acceptance and decrease the appetitive quality
427 of sweet.
428 We were also surprised that small reductions in sweet cell number resulted in such large
429 effects on sweet taste behavior. KIT may therefore have additional functions in taste
430 homeostasis. For example, KIT has known roles within the nervous system. *Kit* mutant mice
431 display learning deficits and decreased synaptic potentiation in the hippocampus (Katafuchi et
432 al., 2000). KIT signaling is also known to modulate synaptic activity between cerebellar Purkinje
433 cells expressing KIT ligand and neighboring KIT^{+} interneurons. (Zaman et al., 2024). KIT may

434 therefore function to modulate signaling between KIT$^+$ taste cells and gustatory neurons. In
435 support of this, transcriptome profiling of gustatory neurons in the geniculate ganglion, which
436 innervate FFP taste buds, revealed expression of both *Kit* and KIT ligand (*Kitl*), suggesting KIT
437 function may be important for proper transmission of taste information to the brain (Zhang et al.,
438 2019, Anderson and Larson, 2020). Additionally, recent findings suggest that KIT function
439 confers resistance to sweet cell loss following nerve injury, and that these residual sweet cells
440 may promote re-innervation of taste buds by regenerating nerve fibers (Ki et al., 2025). Together,
441 these studies suggest that the loss of sweet preference in cabozantinib-treated mice could be due
442 to effects on sweet-sensing gustatory neurons in addition to the effects on type II TBC
443 differentiation.

444 On the other hand, behavioral preferences for bitter and sour tastants were unaffected by
445 TKI treatment. Since GUST expression is associated with bitter cells in both CVP and FFP taste
446 buds (Kim et al., 2003, Tomonari et al., 2011), we expected the increase in GUST$^+$ type II cells
447 to cause hypersensitivity to bitter. However, behavioral sensitivity to bitter compounds may
448 already be maximal. Many plants, fungi, and animals produce toxic or poisonous substances to
449 deter predation; these are almost always bitter, and thus the taste system may have evolved to
450 detect and allow avoidance of bitter substances at low concentrations (Reed and Knaapila, 2010).
451 If bitter taste sensitivity is already high, small increases in bitter cells would have little functional
452 consequence. Overall, our data suggest that loss of sweet taste function is a primary cause of
453 TKI-induced dysgeusia. Intriguingly, sweet taste was reportedly the most commonly affected
454 taste modality in patients treated with TKIs for gastrointestinal stromal tumors, while salt taste
455 was the second most commonly affected taste modality (Van Elst et al., 2022).
456

457 **Limitations and future directions**

458 While TKI treatment decreased sodium-sensing type II cells in FFP taste buds, we did not
459 test salt behavior in TKI-treated mice. FFP sodium TBCs mediate detection of low, appetitive
460 concentrations of salt (Ohmoto et al., 2020). Practically, motivating mice to prefer such low
461 concentrations requires dietary salt depletion that may not be well tolerated by TKI-treated mice
462 (Chandrashekar et al., 2010). Additionally, while the taste system of mice is broadly similar to
463 that of humans (Tizzano et al., 2015), we can only speculate that humans experience similar cell
464 type shifts and changes in taste preferences. This limitation could be addressed in the future by

465 collecting taste bud biopsies from TKI-treated patients to investigate whether cellular changes
466 are similar to those observed in mice, and by performing psychophysical taste testing for
467 individual tastants (Doty, 2019) in patients experiencing dysgeusia.
468 In closing, given the importance of sweet cells in the maintenance of sweet taste
469 preference, and given KIT's role in regulating sweet cell renewal in CVP taste buds, we propose
470 that KIT inhibition contributes to TKI-induced dysgeusia. In addition to the three TKIs tested
471 here, KIT is an off-target RTK of seven anti-angiogenic TKIs currently used in clinical practice
472 (Klaeger et al., 2017, Chang et al., 2022, Sánchez-Gastaldo et al., 2017). Thus, KIT inhibition
473 may underlie dysgeusia in this large class of targeted cancer therapies. For drugs used to treat
474 mRCC, KIT is not an intended target, as therapeutic efficacy relies primarily on VEGFR and
475 PDGFRβ inhibition (Sánchez-Gastaldo et al., 2017). Developing alternatives that maintain
476 inhibition of these targets without inhibiting KIT could alleviate dysgeusia while maintaining
477 efficacy in treating mRCC. There are also cancers in which oncogenic KIT mutations drive
478 tumorigenesis, such as gastrointestinal stromal tumors, melanomas, small cell lung cancer and
479 many leukemias (Lennartsson and Rönnstrand, 2012). Unfortunately, treating these cancers
480 requires KIT inhibition and therefore dysgeusia is likely unavoidable. Developing targeted
481 therapies that specifically inhibit mutated KIT without inhibiting wild-type KIT may mitigate
482 dysgeusia in these cases. By establishing KIT as a regulator of type II TBC subtype renewal and
483 showing that *Kit* knockout underpins the response to TKI treatment, we have provided a
484 promising candidate for future mitigation strategies.
485
486 **Materials and Methods**
487
488 **Animals**
489 Commercially available mice were obtained from the Jackson Laboratory ($Lgr5^{EGFP\text{-}IRES\text{-}CreERT2}$,
490 008875; $Shh^{CReERT2}$, 005623; $Rosa26^{TdTomato}$, 007909; $Rosa26^{YFP}$, 006148; $Pou2F3^{CreERT2\text{-}IRES\text{-}eGFP}$,
491 037511). $Kit^{CreER/+}$;$Rosa26^{YFP/YFP}$ mice were a gift from Stephen W. Santoro, University
492 of Colorado Anschutz Medical Campus, Aurora CO (originally reported (Klein et al., 2013)).
493 $Pou2F3^{CreERT2\text{-}IRES\text{-}eGFP\ /+}$;$Kit^{fl/fl}$ mice were a gift from Jakob von Moltke, University of
494 Washington, Seattle WA (Lara et al. 2025, in revision). Mice were maintained in an AAALAC-
495 accredited facility in compliance with the Guide for Care and Use of Laboratory Animals,

496 Animal Welfare Act, and Public Health Service Policy. Male and female adult mice between 8-
497 20 weeks were used. Procedures were approved by the Institutional Animal Care and Use
498 Committee at the University of Colorado Anschutz Medical Campus.
499
500 **Administration of drugs**
501 Cabozantinib malate (XL 184, SelleckChem) was suspended in HPLC water at 6 mg/ml with 5
502 µl/ml 1N HCL (Fisher Chemical), sonicated for 10 min, heated at 37˚C for 15 min with
503 vortexing, and sonicated for another 10 min. Adult mice on mixed background were individually
504 housed and dosed with 60 mg/kg cabozantinib or vehicle via oral gavage. Mice were weighed
505 daily to monitor health.
506
507 Tamoxifen gavage: Tamoxifen (Sigma-Aldrich) was suspended in corn oil + 10% ETOH at 10
508 mg/ml. Adult mice were individually housed and gavaged with 50 mg/kg
509 ($Shh^{CreER/+};Rosa^{26tdTomato/+}$) or 100 mg/kg ($Kit^{CreER/+};Rosa26^{YFP/YFP}$ and $Pou2F3^{CreER/+};Kit^{fl/fl}$).
510 Cages were changed daily for 7 days after final tamoxifen dose or until mice were harvested,
511 whichever came first.
512
513 Tamoxifen chow: Control ($Kit^{fl/fl}$) and experimental ($Pou2F3^{CreER/+};Kit^{fl/fl}$) mice were
514 individually housed and fed Tamoxifen chow (Inotiv, 500) ad libitum for 4 weeks. Mice were
515 weighed daily for the first 10 days to monitor weight loss, then weighed three times per week for
516 the remainder of the study once their weights recovered and stabilized.
517
518 **Behavioral Assays**
519 Two-bottle taste preference test: Preference for SC45647 was tested in a 48 hr two-bottle
520 behavioral assay (Gaillard and Stratford, 2016). Mice were individually housed in regular
521 ventilated cages with *ad libitum* chow. Graduated bottles were created from cut plastic
522 serological pipettes fitted with a sipper tube on one end and a rubber stopper on the other. Mice
523 were trained for 4 days; first with deionized water in one of 2 bottles, and positions switched
524 after 24 hrs. In the second 2 days, mice had access to water in both bottles. To test sweet taste
525 preference, mice had one bottle of water and one bottle of SC45647 (3 µM in deionized water)
526 for 48 hrs; the volume consumed was measured at 24 hrs, bottles refilled as necessary, and left-

527 right position switched to control for side preference. Sweet preference ratio was calculated by
528 dividing the volume of SC45647 consumed by the sum of the volume of water and SC45647
529 consumed over 48 hrs. This was repeated for 10 μM and 100 μM SC45647.
530
531 Brief Access Test (Lickometer): Three Davis Rig MS-160 lickometers (DiLog Instruments, Inc.,
532 Tallahassee, FL, USA) were used to test taste preference of vehicle- and cabozantinib-treated
533 mice. Detailed protocol and operating procedures have been described fully (Gaillard and
534 Stratford, 2016). During the last 2 weeks of drug or vehicle treatment, mice were trained and
535 tested in one of three lickometers randomly assigned each day. Chamber areas were reduced by
536 half to reduce exploration and distraction from surroundings. Training and test sessions were
537 limited to 30 min. During brief-access testing a shutter opens to give mice access to a bottle of
538 tastant for 5 sec (counted from first lick), the shutter closes for 7.5 sec, and the next bottle is
539 moved into position via an automated mobile rack for the next 5 sec trial. Mice were deprived of
540 water for 23.5 hrs prior to training or testing to motivate drinking. Mice were trained to drink
541 water in the lickometer for 4 consecutive days: For 2 days, the shutter was open and water
542 available for 30 min; then on days 3 and 4, two bottles of water were alternately presented for 5
543 sec each for 30 min. After 2 days of recovery, mice had a final day of training with two
544 alternating bottles of water. Once trained, mice were tested for behavioral taste preference for 4
545 days. For each cabozantinib versus vehicle experiment, only 2 of a total of 3 tastants were
546 assayed, each for 2 days. These included: Sweet - SC45647 (30, 100, 300 and 1000 μM), Bitter -
547 quinine (0.1, 0.3, 1 and 3 mM) and Sour - citric acid (1, 3, 10 and 30 mM). All solutions were
548 made in deionized water. Each test session consisted of up to eight trial blocks (each block
549 comprised five presentations in random order - water and 4 concentrations of one tastant). For
550 sweet SC45647, the first block was not included in our analysis as a thirst-induced high
551 motivational state during the first block may drive maximal licking for all solutions (Gaillard and
552 Stratford, 2016). Mouse thirst for all tastants was calculated from the total licks across the first
553 block averaged across the two testing days. Results of behavior tests are expressed as the lick
554 ratio (average licks to tastant/average licks to water).
555
556 **Tissue Preparation**

557 Mice were euthanized by CO_2 asphyxiation. Tongues were dissected from the lower jaw,
558 incubated for 3 hrs at 4°C in 4% paraformaldehyde (PFA) in 0.1 M phosphate buffer (PB), and
559 placed in sucrose (20% in 0.1 M PB) overnight at 4°C. Samples were embedded in OCT
560 Compound (Tissue-Tek), 12 µm cryosections collected on SuperFrost Plus slides (Thermo Fisher
561 Scientific) and stored at −80°C. For the CVP, 6 sets of 9 sections were collected, while for the
562 FFP, 6 sets of 16 sections were collected.
563
564 **Immunofluorescence**
565 Tissue sections: Sections were washed in 0.1 M PBS, incubated in blocking solution (BS: 5%
566 normal goat or donkey serum, 1% bovine serum albumin, 0.3% Triton X-100 in 0.1 M PBS at
567 pH 7.3) for 1.5 hrs RT followed by primary antibodies (Table S2) diluted in BS overnight at 4°C.
568 Sections were rinsed in PBS + 0.1% Triton, incubated for 1 hr at RT in secondary antibodies in
569 BS, followed by DAPI nuclear counterstaining and washes with 0.1 M PB (Invitrogen;
570 1:10,000). Slides were cover-slipped with ProLong Gold (Thermo Fisher Scientific).
571
572 Organoids: Organoids were generated from taste progenitor cells obtained via FACS of
573 dissociated CVP epithelia from *Lgr5*$^{EGFP\text{-}IRES\text{-}CreERT2}$ mice following our published protocol
574 (Shechtman et al., 2021). To harvest, organoids were incubated in Cell Recovery Solution
575 (Corning) at 4°C, washed in 0.1 M PBS, fixed in 4% PFA and stored at 4°C in PBS with 1%
576 BSA. For immunofluorescence, organoids were incubated in BS (2 hrs), then with primary
577 antibodies (Table S2) in BS for 3 nights at 4°C, washed with PBS + 0.2% Triton and incubated
578 with secondary antibodies in BS overnight at 4°C. Organoid nuclei were counterstained with
579 DAPI, washed with 0.1 M PB and mounted on SuperFrost Plus slides in Fluoromount (Southern
580 Biotech).
581
582 **Hybridization chain reaction RNA-fluorescence *in situ* hybridization**
583 Molecular Instruments designed and produced probes against *Tas1r2* (NM_031873.1),
584 *Kit* (NM_001122733.1) and *Trpm5* (NM_020277.2). Methods were adapted from the
585 manufacturer's protocol. Fixed frozen sections were incubated in 4% PFA for 10 min at RT,
586 washed with 0.1X PBS and incubated in 2 µg/ml Proteinase K for 2 min (CVP) or 5 min (FFP) at
587 RT. Sections were incubated in triethanolamine solution, 12 M HCl and acetic anhydride in

588 DEPC-treated water for 10 min at RT, washed with 0.1X PBS, incubated in hybridization buffer
589 for 45 min at 37°C, and then with 1.2 pmol (CVP) or 1.5 pmol (FFP) probe in hybridization
590 buffer overnight at 37°C. Sections were washed with 75% wash buffer/25% 5× SSCT (20× SSC
591 and 10% Tween20, ultrapure water), 50% wash buffer/50% 5× SSCT, 25% wash buffer/75% 5×
592 SSCT, and 100% 5× SSCT, each for 20 min at 37°C, then with 100% 5× SSCT for 20 min at RT.
593 Sections were incubated in amplification buffer for 1 hr, then in denatured hairpin solution (6
594 pmol hairpin 1 and 2 in amplification buffer) overnight. Slides were washed with 5× SSCT,
595 nuclei counterstained with DAPI, washed with 0.1 M PB and cover-slipped with ProLong Gold.
596

597 **Organoid Derivation**

598 Organoids were derived according to our published protocol (Shechtman et al., 2021).
599 For each experiment, organoids were derived from CVP epithelium from 3-6 *Lgr5*$^{EGFP\text{-}IRES\text{-}}$
600 ^{CreERT2} mice aged 8-20 weeks. Briefly, collagenase (2 mg/ml) and dispase (5 mg/ml) in
601 phosphate-buffered saline (PBS) were injected around the CVP, then the epithelium peeled and
602 dissociated for 45 min in collagenase (2 mg/ml), dispase (5 mg/ml) and elastase (2 mg/ml) at
603 37°C. Cells were centrifuged (320 ***g*** at 4°C), the pellet resuspended in FACS buffer [1 mM
604 EDTA, 25 mM HEPES (pH 7.0), 1% FBS, 1×Ca^{2+}/Mg^{2+}-free dPBS], passed through a 30 µm
605 cell strainer, stained with DAPI (Thermo Fisher Scientific) and subjected to FACS on a MoFlo
606 XDP100 (Cytomation). Debris and doublets were gated out via side-scatter (FSC and SSC-width,
607 respectively), live (DAPI^{neg}) cells were enriched, and the gating of GFP^{+} signal was determined
608 relative to background fluorescence of epithelial cells from a wild-type control mouse processed
609 in parallel (see (Shechtman et al., 2021) for gating strategy). Only *Lgr5*-GFP^{+} cells were
610 collected. Sorted GFP^{+} cells were plated in 48-well plates at 200 cells/well in 15 µl Matrigel and
611 grown in WENR+AS media to support growth (days 0-6) and WENR media to promote TBC
612 differentiation (days 6-12). WENR: 50% WRN (WNT/RSPO/Noggin)-conditioned media
613 (Miyoshi and Stappenbeck, 2013) plus 1× Glutamax (Gibco), 1× HEPES (Gibco), 1× penicillin-
614 streptomycin (Gibco), 1× B27 supplement (Gibco), 1× gentamicin (Gibco), 1× primocin
615 (InvivoGen), 25 ng/ml murine Noggin (Peprotech), 50 ng/ml murine EGF (Peprotech), 1 mM
616 nicotinamide (Sigma), and 1 mM N-acetyl-L-cysteine (Sigma). WENR+AS: WENR plus 500
617 nM A83-01 (Sigma) and 0.4 µM SB202190 (R&D Systems). Y27632 (10 µm; Stemgent) was
618 added on days 0-2 to promote cell survival.

619

620 Drug treatment: cabozantinib (SelleckChem; S4001), axitinib (SelleckChem; S1005), sunitinib
621 (SelleckChem; S7781), and paclitaxel (SelleckChem; S1150) were dissolved in DMSO to a stock
622 concentration of 50 µM, and diluted in organoid media (WENR+AS or WENR depending on the
623 experiment) to a final concentration of 50 nM or 100 nM. For controls, the same volume of
624 DMSO used for 100 nM drug was added to organoid media. Medium was changed every 2 days.
625

626 **Quantitative RT-PCR**

627 Organoids were harvested as described (Shechtman et al., 2021). Briefly, plates were
628 placed on ice for 30 min and organoids freed from Matrigel by scratching with a pipet tip.
629 Organoid samples were centrifuged and resuspended in RLT buffer (Qiagen) with 1% β-
630 mercaptoethanol. RNA was extracted using a RNeasy Micro Kit (Qiagen), quantified via
631 Nanodrop (Thermo Fisher Scientific) and reverse transcribed with an iScript cDNA synthesis kit
632 (Bio-Rad). Power SYBR Green PCR Master Mix (Applied Biosystems) was used for qPCR
633 reactions on a StepOne Plus Real-Time PCR System (Applied Biosystems, Life Technologies).
634 Relative gene expression was assessed using the ΔΔCT method (Livak and Schmittgen, 2001),
635 with *Rpl19* as the housekeeping gene. Primers are listed in **Table S1**. Organoids from three wells
636 of a 48-well plate were pooled per RNA sample and three samples were collected per experiment
637 for RT-qPCR.
638

639 **EdU incubation, detection and quantification**

640 Organoids were grown in 48-well plates as described above and on day 6, EdU (4 mM
641 stock in 0.9% NaCl) was added to WENR+AS media at a final concentration of 10 µM for 30
642 min. Cultures were placed in fresh WENR+AS on ice and organoids harvested for
643 immunofluorescence as above. A Click-it® EdU Alexa Fluor® 647 Imaging Kit (Invitrogen)
644 was used to detect EdU signal using methods adapted from the manufacturer's protocol.
645 Organoids were washed with PBS +0.2% Triton, washed with PBS + 0.1% BSA, then incubated
646 in Click-it® Plus reaction cocktail for 3 hrs at RT. Organoids were washed with PBS, nuclei
647 counterstained with DAPI, washed with 0.1 M PB and mounted on SuperFrost Plus slides in
648 Fluoromount (Southern Biotech). Using a custom app - OrganoidAnalyzer in MATLAB 2024a
649 (Mathworks, Natick, MA) (https://github.com/salcedoe/OrganoidAnalysis) - we determined the

650 ratio of EdU^+ pixels to total $DAPI^+$ pixels in each organoid. See supplemental materials for
651 details.
652 This app allows the user to select and open a confocal image stack and visually inspect
653 each stack by channel and optical section. The app also provides the controls to process and
654 segment the stack, and capture and collate the data. The app uses the Bio-Formats MATLAB
655 toolbox (Linkert et al., 2010) to open each image stack. Once a confocal z-stack is opened, each
656 channel in the stack is processed separately. Image stacks are normalized to the maximum
657 intensity found in the channel (using the **mat2gray** function). Stacks are then filtered using a
658 median filter with the default neighborhood settings (**medfilt3**) and a gaussian filter using a 5 x 5
659 x 5 filter size (**imgaussfilt3**). To increase contrast and enhance separation between nuclei in an
660 organoid, we create an image stack marker by applying an erosion morphological operation on
661 the filtered stack (**imerode)** using a sphere-shaped structuring element with a radius of 3 voxels
662 (**strel**). We then perform a morphological reconstruction of the filtered volume using the image
663 stack marker we created in the previous step (**imreconstruct)**. To identify labeled nuclei, image
664 stacks are segmented into labeled nuclei and background using a modified version of Otsu's
665 Method for thresholding. Specifically, a threshold value is calculated for each channel using
666 **graythresh** and this value is multiplied by a set factor (i.e. 0.5 for the DAPI channel and 0.2 for
667 the EdU channel). The same factors are used for all image stacks to ensure consistent
668 segmentation. To create the binarized segmentation image stack, pixels with intensity values
669 greater than the threshold value are labeled with a logical one to signify labeled cells, while
670 pixels with intensity values below the threshold value are labeled with logical zeros to signify
671 background. We created two separate segmentation stacks: one for the EdU-labeled cells and one
672 for the DAPI-labeled cells. Each segmentation stack is visually inspected and compared to the
673 original image stack to ensure that pixels designated as signal were in fact signal and not noise.
674 The ratio of EdU^+ nuclei to total $DAPI^+$ nuclei was calculated by dividing the total number of
675 logical ones in the EdU binarized image stack by the total number of logical ones in the DAPI
676 binarized image stack. As such, we are in effect dividing the total volume of EdU^+ nuclei by the
677 total volume of all $DAPI^+$ nuclei to calculate the ratio. This was necessary as our technique was
678 unable to separate all individual nuclei in an organoid, especially the $DAPI^+$ nuclei which are
679 tightly clustered together.
680

681 **Cell-Titer Glo® 3D**

682 Organoids were derived and cultured as above but in opaque-walled 96-well plates at 100 cells
683 per well in 3 µl Matrigel. On day 6, plates were equilibrated to RT for 30 min, after which an
684 equal volume of Cell-Titer Glo® 3D reagent (Promega) was added to cultures (150 µl
685 WENR+AS with drugs or DMSO + 150 µl reagent in each well). Plates were mixed on an
686 automatic plate shaker for 5 min to induce cell lysis. Luminescence was recorded after 25 min
687 using a Synergy H1 microplate reader (BioTek). The average luminescence across 6 wells was
688 calculated for each condition in each biological replicate.

689

690 **Image acquisition and analysis**

691 Immunofluorescence: Tissue sections and organoids were imaged with a Leica TCS SP8 laser-
692 scanning confocal microscope with LAS X software. *Z*-stacks of optical sections of CVP and
693 FFP sections were acquired at 0.75 µm thickness, and organoids at 2 µm optical section
694 thickness. For image acquisition, analysis, and cell counts using LAS X Office software,
695 investigators were blinded to condition. For CVP, all taste buds in 5 tissue sections were
696 counted. For FFP, all taste buds in 16 sections from the tongue tip were counted. Criteria for
697 immunolabeled cell counts: (1) cell is immunomarker-positive; and (2) has a $DAPI^+$ nucleus.
698 Taste buds were identified during cell counting using either PLCβ2 staining (co-staining with
699 GUST and YFP), KRT8 staining (co-staining with SNAP25 and KIT), or *Trpm5* HCR *in-situ*
700 hybridization (with *Tas1r2* probe).

701

702 Taste bud area: Maximum z-stack projections of KRT8 immunofluorescence tissue sections were
703 generated and imported into ImageJ software. A scalebar was used to set pixels/µm scale.
704 Individual taste buds were outlined using the Freehand Selection tool to obtain the area of each
705 taste bud profile.

706

707 **Statistical analyses**

708 In experiments with two conditions, normally distributed data were analyzed by unpaired
709 t-test, and Mann-Whitney U tests were used when data were not normally distributed. In
710 experiments with more than two conditions, normally distributed data were analyzed by ordinary
711 one- or two-way ANOVA with either Sidak's or Tukey's multiple comparisons post-hoc test. A

712 Kruskal-Wallis comparison test was used when data were not normally distributed. All statistical
713 analyses employed GraphPad Prism software. Data plotted throughout are depicted as Mean ±
714 S.E.M. and significance was taken as $p<0.05$ with a confidence interval of 95%.
715

716 **Acknowledgments**

717 The authors thank the University of Colorado Organoid and Tissue Modeling Shared Resource
718 (OTMSR) for providing WRN conditioned media and technical assistance for organoid
719 experiments. The authors thank Dmitry Baturin and Lester Acosta of the University of Colorado
720 Cancer Center Flow Cytometry Shared Resource for FACS, Trevor J. Isner and Amanda Stenzel
721 for technical assistance with mouse and organoid experiments, and Thomas E. Finger, Katherine
722 Fantauzzo, Heide Ford, Stephen Santoro, Santos Franco, Trevor J. Isner and Ian J. Purvis for
723 helpful discussions and for critically reading the manuscript. Finally, we heartily thank Robin F.
724 Krimm for sharing unpublished data.
725

726 **Funding:**

727 National Institutes of Health T32GM141742 (CMP)
728 National Institutes of Health F31DC020634-01 (CMP)
729 National Institutes of Health R01DC021865 (LAB)
730 National Institutes of Health R01DC018489 (LAB)
731 National Institutes of Health R01DC012383 (LAB)
732 National Institutes of Health R21CA236480 (LAB)
733 National Institutes of Health R01AI167923 (JVM)
734 National Institutes of Health P30CA046934 (CU OTMSR)
735 National Institutes of Health P30DK116073 (CU OTMSR)
736 National Institutes of Health P30CA046934 (CU Cancer Center)
737

738 **Author contributions:**

739 Project conceptualization: CMP, LAB, PJD, ETL
740 Organoid experiments: CMP, JKS
741 MATLAB coding and custom app creation: ES
742 Mouse handling: CMP, JKS, CEW

743 Tissue processing: CMP, JKS, ASH

744 Imaging and cell counting: CMP, ASH

745 Behavior: CMP, CEW, ASH

746 Generation of novel KIT10 allele: HIL, JVM

747 Writing: CMP, ES, LAB

748 Figure creation: CMP, LAB

749 Editing: all authors

750

751 **Competing interests:** Authors declare that they have no competing interests.

752

753 **Data and materials availability:** All relevant data and details of resources can be found within
754 the article and its supplementary information.

755

756 **References:**

757 **Anderson, C. B. & Larson, E. D.** 2020. Single cell transcriptional profiling of phox2b-
758 expressing geniculate ganglion neurons. *bioRxiv*, 812578.
759 **Barlow, L. A.** 2015. Progress and renewal in gustation: New insights into taste bud
760 development. *Development,* 142, 3620-9.
761 **Bartel, D. L., Sullivan, S. L., Lavoie, É. G., Sévigny, J. & Finger, T. E.** 2006. Nucleoside
762 triphosphate diphosphohydrolase-2 is the ecto-atpase of type i cells in taste buds. *Journal*
763 *of Comparative Neurology,* 497, 1-12.
764 **Beidler, L. M. & Smallman, R. L.** 1965. Renewal of cells within taste buds. *J Cell Biol,* 27,
765 263-72.
766 **Biggs, B. T., Tang, T. & Krimm, R. F.** 2016. Insulin-like growth factors are expressed in the
767 taste system, but do not maintain adult taste buds. *PLoS One,* 11, e0148315.
768 **Castillo-Azofeifa, D., Losacco, J. T., Salcedo, E., Golden, E. J., Finger, T. E. & Barlow, L.**
769 **A.** 2017. Sonic hedgehog from both nerves and epithelium is a key trophic factor for taste
770 bud maintenance. *Development,* 144, 3054-3065.
771 **Castillo, D., Seidel, K., Salcedo, E., Ahn, C., De Sauvage, F. J., Klein, O. D. & Barlow, L. A.**
772 2014. Induction of ectopic taste buds by shh reveals the competency and plasticity of
773 adult lingual epithelium. *Development,* 141, 2993-3002.
774 **Chandrashekar, J., Kuhn, C., Oka, Y., Yarmolinsky, D. A., Hummler, E., Ryba, N. J. &**
775 **Zuker, C. S.** 2010. The cells and peripheral representation of sodium taste in mice.
776 *Nature,* 464, 297-301.
777 **Chandrashekar, J., Yarmolinsky, D., Von Buchholtz, L., Oka, Y., Sly, W., Ryba, N. J. &**
778 **Zuker, C. S.** 2009. The taste of carbonation. *Science,* 326, 443-5.
779 **Chang, E., Weinstock, C., Zhang, L., Fiero, M. H., Zhao, M., Zahalka, E., Ricks, T. K.,**
780 **Fourie Zirkelbach, J., Qiu, J., Yu, J., Chen, X. H., Bhatnagar, V., Goldberg, K. B.,**
781 **Tang, S., Kluetz, P. G., Pazdur, R., Ibrahim, A., Beaver, J. A. & Amiri-Kordestani,**

782 **L.** 2022. Fda approval summary: Tivozanib for relapsed or refractory renal cell
783 carcinoma. *Clin Cancer Res,* 28**,** 441-445.
784 **Choo, E. & Dando, R.** 2021. The c-kit receptor tyrosine kinase marks sweet or umami sensing
785 t1r3 positive adult taste cells in mice. *Chemosensory Perception,* 14**,** 41-46.
786 **Clapp, T. R., Yang, R., Stoick, C. L., Kinnamon, S. C. & Kinnamon, J. C.** 2004.
787 Morphologic characterization of rat taste receptor cells that express components of the
788 phospholipase c signaling pathway. *Journal of Comparative Neurology,* 468**,** 311-321.
789 **Davis, M. I., Hunt, J. P., Herrgard, S., Ciceri, P., Wodicka, L. M., Pallares, G., Hocker, M.,**
790 **Treiber, D. K. & Zarrinkar, P. P.** 2011. Comprehensive analysis of kinase inhibitor
791 selectivity. *Nature Biotechnology,* 29**,** 1046-1051.
792 **Delay, R. J., Roper, S. D. & Kinnamon, J. C.** 1986. Ultrastructure of mouse vallate taste buds:
793 Ii. Cell types and cell lineage. *Journal of Comparative Neurology,* 253**,** 242-252.
794 **Donnelly, C. R., Shah, A. A., Mistretta, C. M., Bradley, R. M. & Pierchala, B. A.** 2018.
795 Biphasic functions for the gdnf-ret signaling pathway in chemosensory neuron
796 development and diversification. *Proc Natl Acad Sci U S A,* 115**,** E516-e525.
797 **Doty, R. L.** 2019. Chapter 15 - psychophysical testing of smell and taste function. *In:* DOTY, R.
798 L. (ed.) *Handbook of clinical neurology.* Elsevier.
799 **Dvoryanchikov, G., Sinclair, M. S., Perea-Martinez, I., Wang, T. & Chaudhari, N.** 2009.
800 Inward rectifier channel, romk, is localized to the apical tips of glial-like cells in mouse
801 taste buds. *Journal of Comparative Neurology,* 517**,** 1-14.
802 **Epstein, J. B. & Barasch, A.** 2010. Taste disorders in cancer patients: Pathogenesis, and
803 approach to assessment and management. *Oral Oncol,* 46**,** 77-81.
804 **Farbman, A. I.** 1969. Fine structure of degenerating taste buds after denervation. *Development,*
805 22**,** 55-68.
806 **Finger, T. E. & Silver, W. L.** 2000. Cell biology of taste epithelium. *In:* FINGER, T. E.,
807 SILVER, W. L. & RESTREPO, D. (eds.) *The neurobiology of taste and smell.* New
808 York: Wiley-Liss.
809 **Gaillard, D. & Barlow, L. A.** 2021. A mechanistic overview of taste bud maintenance and
810 impairment in cancer therapies. *Chem Senses,* 46.
811 **Gaillard, D., Bowles, S. G., Salcedo, E., Xu, M., Millar, S. E. & Barlow, L. A.** 2017. B-
812 catenin is required for taste bud cell renewal and behavioral taste perception in adult
813 mice. *PLoS Genet,* 13**,** e1006990.
814 **Gaillard, D., Shechtman, L. A., Millar, S. E. & Barlow, L. A.** 2019. Fractionated head and
815 neck irradiation impacts taste progenitors, differentiated taste cells, and wnt/β-catenin
816 signaling in adult mice. *Sci Rep,* 9**,** 17934.
817 **Gaillard, D. & Stratford, J. M.** 2016. Measurement of behavioral taste responses in mice: Two-
818 bottle preference, lickometer, and conditioned taste-aversion tests. *Current protocols in*
819 *mouse biology,* 6**,** 380-407.
820 **Gerbe, F., Sidot, E., Smyth, D. J., Ohmoto, M., Matsumoto, I., Dardalhon, V., Cesses, P.,**
821 **Garnier, L., Pouzolles, M., Brulin, B., Bruschi, M., Harcus, Y., Zimmermann, V. S.,**
822 **Taylor, N., Maizels, R. M. & Jay, P.** 2016. Intestinal epithelial tuft cells initiate type 2
823 mucosal immunity to helminth parasites. *Nature,* 529**,** 226-30.
824 **Golden, E. J., Larson, E. D., Shechtman, L. A., Trahan, G. D., Gaillard, D., Fellin, T. J.,**
825 **Scott, J. K., Jones, K. L. & Barlow, L. A.** 2021. Onset of taste bud cell renewal starts at
826 birth and coincides with a shift in shh function. *Elife,* 10.

827 **Hahn, A. W., Klaassen, Z., Agarwal, N., Haaland, B., Esther, J., Ye, X. Y., Wang, X., Pal,**
828 **S. K. & Wallis, C. J. D.** 2019. First-line treatment of metastatic renal cell carcinoma: A
829 systematic review and network meta-analysis. *Eur Urol Oncol,* 2**,** 708-715.
830 **Halpage, J., Dasilva Pantoja, P. & Mancarella, S.** 2024. Prolonged tamoxifen-enriched diet is
831 associated with cardiomyopathy and nutritional frailty in mice. *Exp Physiol,* 109**,** 513-
832 523.
833 **Hamazaki, R. & Uesawa, Y.** 2024. Characterization of antineoplastic agents inducing taste and
834 smell disorders using the faers database. *Pharmaceuticals (Basel),* 17.
835 **Hirose, F., Takai, S., Takahashi, I. & Shigemura, N.** 2020. Expression of protocadherin-20 in
836 mouse taste buds. *Sci Rep,* 10**,** 2051.
837 **Hsu, C.-C., Seta, Y., Matsuyama, K., Kataoka, S., Nakatomi, M., Toyono, T., Gunjigake, K.**
838 **K., Kuroishi, K. N. & Kawamoto, T.** 2021. Mash1-expressing cells may be relevant to
839 type iii cells and a subset of plcβ2-positive cell differentiation in adult mouse taste buds.
840 *Cell and Tissue Research,* 383**,** 667-675.
841 **Iwasaki, S., Aoyagi, H. & Yoshizawa, H.** 2011. Localization of keratins 13 and 14 in the
842 lingual mucosa of rats during the morphogenesis of circumvallate papillae. *Acta*
843 *Histochem,* 113**,** 395-401.
844 **Jewkes, B. C., Barlow, L. A. & Delay, E. R.** 2018. Effect of radiation on sucrose detection
845 thresholds of mice. *Chemical senses,* 43**,** 53-58.
846 **Karaman, M. W., Herrgard, S., Treiber, D. K., Gallant, P., Atteridge, C. E., Campbell, B.**
847 **T., Chan, K. W., Ciceri, P., Davis, M. I., Edeen, P. T., Faraoni, R., Floyd, M., Hunt,**
848 **J. P., Lockhart, D. J., Milanov, Z. V., Morrison, M. J., Pallares, G., Patel, H. K.,**
849 **Pritchard, S., Wodicka, L. M. & Zarrinkar, P. P.** 2008. A quantitative analysis of
850 kinase inhibitor selectivity. *Nature Biotechnology,* 26**,** 127-132.
851 **Katafuchi, T., Li, A.-J., Hirota, S., Kitamura, Y. & Hori, T.** 2000. Impairment of spatial
852 learning and hippocampal synaptic potentiation in c-kit mutant rats. *Learning & Memory,*
853 7**,** 383-392.
854 **Kataoka, S., Yang, R., Ishimaru, Y., Matsunami, H., Sévigny, J., Kinnamon, J. C. &**
855 **Finger, T. E.** 2008. The candidate sour taste receptor, pkd2l1, is expressed by type iii
856 taste cells in the mouse. *Chemical senses,* 33**,** 243-254.
857 **Ki, S. Y., Jang, J. H., Kim, D. H. & Jeong, Y. T.** 2025. C-kit signaling confers damage-
858 resistance to sweet taste cells upon nerve injury. *Int J Oral Sci,* 17**,** 57.
859 **Kim, M.-R., Kusakabe, Y., Miura, H., Shindo, Y., Ninomiya, Y. & Hino, A.** 2003. Regional
860 expression patterns of taste receptors and gustducin in the mouse tongue. *Biochemical*
861 *and Biophysical Research Communications,* 312**,** 500-506.
862 **Kinnamon, J. C.** 1991. Organization and innervation of taste buds. *In:* FINGER, T. E. &
863 SILVER, W. L. (eds.) *The neurobiology of taste and smell.* Krieger Publishing Company.
864 **Kinnamon, J. C., Henzler, D. M. & Royer, S. M.** 1993. Hvem ultrastructural analysis of mouse
865 fungiform taste buds, cell types, and associated synapses. *Microscopy research and*
866 *technique,* 26**,** 142-156.
867 **Kiselyov, A., Balakin, K. V. & Tkachenko, S. E.** 2007. Vegf/vegfr signalling as a target for
868 inhibiting angiogenesis. *Expert Opin Investig Drugs,* 16**,** 83-107.
869 **Klaeger, S., Heinzlmeir, S., Wilhelm, M., Polzer, H., Vick, B., Koenig, P. A., Reinecke, M.,**
870 **Ruprecht, B., Petzoldt, S., Meng, C., Zecha, J., Reiter, K., Qiao, H., Helm, D., Koch,**
871 **H., Schoof, M., Canevari, G., Casale, E., Depaolini, S. R., Feuchtinger, A., Wu, Z.,**
872 **Schmidt, T., Rueckert, L., Becker, W., Huenges, J., Garz, A. K., Gohlke, B. O., Zolg,**

D. P., Kayser, G., Vooder, T., Preissner, R., Hahne, H., Tõnisson, N., Kramer, K., Götze, K., Bassermann, F., Schlegl, J., Ehrlich, H. C., Aiche, S., Walch, A., Greif, P. A., Schneider, S., Felder, E. R., Ruland, J., Médard, G., Jeremias, I., Spiekermann, K. & Kuster, B. 2017. The target landscape of clinical kinase drugs. *Science,* 358.

Klein, S., Seidler, B., Kettenberger, A., Sibaev, A., Rohn, M., Feil, R., Allescher, H.-D., Vanderwinden, J.-M., Hofmann, F., Schemann, M., Rad, R., Storr, M. A., Schmid, R. M., Schneider, G. & Saur, D. 2013. Interstitial cells of cajal integrate excitatory and inhibitory neurotransmission with intestinal slow-wave activity. *Nature Communications,* 4**,** 1630.

Koch, S., Tugues, S., Li, X., Gualandi, L. & Claesson-Welsh, L. 2011. Signal transduction by vascular endothelial growth factor receptors. *Biochemical Journal,* 437**,** 169-183.

Krishnamoorthy, N., Oriss, T. B., Paglia, M., Fei, M., Yarlagadda, M., Vanhaesebroeck, B., Ray, A. & Ray, P. 2008. Activation of c-kit in dendritic cells regulates t helper cell differentiation and allergic asthma. *Nat Med,* 14**,** 565-73.

Kumari, A., Ermilov, A. N., Allen, B. L., Bradley, R. M., Dlugosz, A. A. & Mistretta, C. M. 2015. Hedgehog pathway blockade with the cancer drug lde225 disrupts taste organs and taste sensation. *J Neurophysiol,* 113**,** 1034-40.

Kumari, A., Yokota, Y., Li, L., Bradley, R. M. & Mistretta, C. M. 2018. Species generalization and differences in hedgehog pathway regulation of fungiform and circumvallate papilla taste function and somatosensation demonstrated with sonidegib. *Sci Rep,* 8**,** 16150.

Lacy, S. A., Miles, D. R. & Nguyen, L. T. 2017. Clinical pharmacokinetics and pharmacodynamics of cabozantinib. *Clin Pharmacokinet,* 56**,** 477-491.

Lee, H., Macpherson, L. J., Parada, C. A., Zuker, C. S. & Ryba, N. J. P. 2017. Rewiring the taste system. *Nature,* 548**,** 330-333.

Lennartsson, J. & Rönnstrand, L. 2012. Stem cell factor receptor/c-kit: From basic science to clinical implications. *Physiological Reviews,* 92**,** 1619-1649.

Li, M., Naqvi, N., Yahiro, E., Liu, K., Powell, P. C., Bradley, W. E., Martin, D. I., Graham, R. M., Dell'italia, L. J. & Husain, A. 2008. C-kit is required for cardiomyocyte terminal differentiation. *Circulation research,* 102**,** 677-685.

Liao, C. P., Booker, R. C., Morrison, S. J. & Le, L. Q. 2017. Identification of hair shaft progenitors that create a niche for hair pigmentation. *Genes Dev,* 31**,** 744-756.

Liman, E. R., Zhang, Y. V. & Montell, C. 2014. Peripheral coding of taste. *Neuron,* 81**,** 984-1000.

Linkert, M., Rueden, C. T., Allan, C., Burel, J.-M., Moore, W., Patterson, A., Loranger, B., Moore, J., Neves, C., Macdonald, D., Tarkowska, A., Sticco, C., Hill, E., Rossner, M., Eliceiri, K. W. & Swedlow, J. R. 2010. Metadata matters: Access to image data in the real world. *Journal of Cell Biology,* 189**,** 777-782.

Liu, H. X., Ermilov, A., Grachtchouk, M., Li, L., Gumucio, D. L., Dlugosz, A. A. & Mistretta, C. M. 2013. Multiple shh signaling centers participate in fungiform papilla and taste bud formation and maintenance. *Dev Biol,* 382**,** 82-97.

Livak, K. J. & Schmittgen, T. D. 2001. Analysis of relative gene expression data using real-time quantitative pcr and the 2(-delta delta c(t)) method. *Methods,* 25**,** 402-8.

Lu, W. J., Mann, R. K., Nguyen, A., Bi, T., Silverstein, M., Tang, J. Y., Chen, X. & Beachy, P. A. 2018. Neuronal delivery of hedgehog directs spatial patterning of taste organ regeneration. *Proc Natl Acad Sci U S A,* 115**,** E200-e209.

919 **Matsumoto, I., Ohmoto, M., Narukawa, M., Yoshihara, Y. & Abe, K.** 2011. Skn-1a (pou2f3)
920 specifies taste receptor cell lineage. *Nature neuroscience,* 14**,** 685-687.
921 **Matsuyama, K., Takai, S., Shigemura, N., Nakatomi, M., Kawamoto, T., Kataoka, S.,**
922 **Toyono, T. & Seta, Y.** 2023. Ascl1-expressing cell differentiation in initially developed
923 taste buds and taste organoids. *Cell and Tissue Research,* 392**,** 631-641.
924 **Mcginty, J. W., Ting, H.-A., Billipp, T. E., Nadjsombati, M. S., Khan, D. M., Barrett, N. A.,**
925 **Liang, H.-E., Matsumoto, I. & Von Moltke, J.** 2020. Tuft-cell-derived leukotrienes
926 drive rapid anti-helminth immunity in the small intestine but are dispensable for anti-
927 protist immunity. *Immunity,* 52**,** 528-541.e7.
928 **Mclaughlin, S. K.** 2000. Erb and c-kit receptors have distinctive patterns of expression in adult
929 and developing taste papillae and taste buds. *J Neurosci,* 20**,** 5679-88.
930 **Miura, H., Kusakabe, Y. & Harada, S.** 2006. Cell lineage and differentiation in taste buds.
931 *Archives of histology and cytology,* 69**,** 209-225.
932 **Miura, H., Scott, J. K., Harada, S. & Barlow, L. A.** 2014. Sonic hedgehog-expressing basal
933 cells are general post-mitotic precursors of functional taste receptor cells. *Dev Dyn,* 243**,**
934 1286-97.
935 **Miyoshi, H. & Stappenbeck, T. S.** 2013. In vitro expansion and genetic modification of
936 gastrointestinal stem cells in spheroid culture. *Nat Protoc,* 8**,** 2471-82.
937 **Moss, K. G., Toner, G. C., Cherrington, J. M., Mendel, D. B. & Laird, A. D.** 2003. Hair
938 depigmentation is a biological readout for pharmacological inhibition of kit in mice and
939 humans. *J Pharmacol Exp Ther,* 307**,** 476-80.
940 **Mukherjee, N., Pal Choudhuri, S., Delay, R. J. & Delay, E. R.** 2017. Cellular mechanisms of
941 cyclophosphamide-induced taste loss in mice. *PLoS One,* 12**,** e0185473.
942 **Nasimi, M., Jorsaraei, S. G. A., Fattahi, E., Tabari, M. G. & Neyshaburi, E. Z.** 2021. Scf
943 improves in vitro differentiation of sscs through transcriptionally up-regulating prtm1,
944 stra8, c-kit, piwil2, and oct4 genes. *Reprod Sci,* 28**,** 963-972.
945 **Nelson, G., Hoon, M. A., Chandrashekar, J., Zhang, Y., Ryba, N. J. & Zuker, C. S.** 2001.
946 Mammalian sweet taste receptors. *Cell,* 106**,** 381-90.
947 **Ninomiya, Y., Kajiura, H. & Mochizuki, K.** 1993. Differential taste responses of mouse
948 chorda tympani and glossopharyngeal nerves to sugars and amino acids. *Neurosci Lett,*
949 163**,** 197-200.
950 **Nofre, C., Tinti, J. M. & Chatzapoulos, F. O.** 1990. *Sweetening agents*. United States patent
951 application.
952 **Nomura, K., Nakanishi, M., Ishidate, F., Iwata, K. & Taruno, A.** 2020. All-electrical ca(2+)-
953 independent signal transduction mediates attractive sodium taste in taste buds. *Neuron,*
954 106**,** 816-829.e6.
955 **Ogata, T. & Ohtubo, Y.** 2020. Quantitative analysis of taste bud cell numbers in the
956 circumvallate and foliate taste buds of mice. *Chem Senses,* 45**,** 261-273.
957 **Ohmoto, M., Jyotaki, M., Foskett, J. K. & Matsumoto, I.** 2020. Sodium–taste cells require
958 skn-1a for generation and share molecular features with sweet, umami, and bitter taste
959 cells. *eneuro,* 7**,** ENEURO.0385-20.2020.
960 **Ohtubo, Y. & Yoshii, K.** 2011. Quantitative analysis of taste bud cell numbers in fungiform and
961 soft palate taste buds of mice. *Brain Res,* 1367**,** 13-21.
962 **Peng, B., Lloyd, P. & Schran, H.** 2005. Clinical pharmacokinetics of imatinib. *Clin*
963 *Pharmacokinet,* 44**,** 879-94.

964 **Perea-Martinez, I., Nagai, T. & Chaudhari, N.** 2013. Functional cell types in taste buds have
965 distinct longevities. *PloS one,* 8**,** e53399.
966 **Piarowski, C. M., Isner, T. J. & Barlow, L. A.** 2025. Developing and regenerating a sense of
967 taste. *Current topics in developmental biology.* Academic Press.
968 **Raica, M. & Cimpean, A. M.** 2010. Platelet-derived growth factor (pdgf)/pdgf receptors (pdgfr)
969 axis as target for antitumor and antiangiogenic therapy. *Pharmaceuticals (Basel),* 3**,** 572-
970 599.
971 **Reed, D. R. & Knaapila, A.** 2010. Genetics of taste and smell: Poisons and pleasures. *Prog Mol*
972 *Biol Transl Sci,* 94**,** 213-40.
973 **Ren, W., Aihara, E., Lei, W., Gheewala, N., Uchiyama, H., Margolskee, R. F., Iwatsuki, K.**
974 **& Jiang, P.** 2017. Transcriptome analyses of taste organoids reveal multiple pathways
975 involved in taste cell generation. *Sci Rep,* 7**,** 4004.
976 **Ren, W., Cha, X., Xu, R., Wang, T., Liang, C., Chou, J., Zhang, X., Li, F., Wang, S., Cai,**
977 **B., Jiang, P., Wang, H., Liu, H. & Yu, Y.** 2023. Cisplatin attenuates taste cell
978 homeostasis and induces inflammatory activation in the circumvallate papilla.
979 *Theranostics,* 13**,** 2896-2913.
980 **Ren, W., Lewandowski, B. C., Watson, J., Aihara, E., Iwatsuki, K., Bachmanov, A. A.,**
981 **Margolskee, R. F. & Jiang, P.** 2014. Single lgr5- or lgr6-expressing taste
982 stem/progenitor cells generate taste bud cells ex vivo. *Proc Natl Acad Sci U S A,* 111**,**
983 16401-6.
984 **Roberto, M., Botticelli, A., Panebianco, M., Aschelter, A. M., Gelibter, A., Ciccarese, C.,**
985 **Minelli, M., Nuti, M., Santini, D., Laghi, A., Tomao, S. & Marchetti, P.** 2021.
986 Metastatic renal cell carcinoma management: From molecular mechanism to clinical
987 practice. *Frontiers in oncology,* 11**,** 657639-657639.
988 **Sánchez-Gastaldo, A., Kempf, E., González Del Alba, A. & Duran, I.** 2017. Systemic
989 treatment of renal cell cancer: A comprehensive review. *Cancer Treatment Reviews,* 60**,**
990 77-89.
991 **Sánchez-Lara, K., Sosa-Sánchez, R., Green-Renner, D., Rodríguez, C., Laviano, A.,**
992 **Motola-Kuba, D. & Arrieta, O.** 2010. Influence of taste disorders on dietary behaviors
993 in cancer patients under chemotherapy. *Nutrition journal,* 9**,** 15-15.
994 **Schaum, N., Karkanias, J., Neff, N. F., May, A. P., Quake, S. R., Wyss-Coray, T.,**
995 **Darmanis, S., Batson, J., Botvinnik, O., Chen, M. B., et al.** 2018. Single-cell
996 transcriptomics of 20 mouse organs creates a tabula muris. *Nature,* 562**,** 367-372.
997 **Seta, Y., Oda, M., Kataoka, S., Toyono, T. & Toyoshima, K.** 2011. Mash1 is required for the
998 differentiation of aadc-positive type iii cells in mouse taste buds. *Dev Dyn,* 240**,** 775-84.
999 **Seta, Y., Stoick-Cooper, C. L., Toyono, T., Kataoka, S., Toyoshima, K. & Barlow, L. A.**
1000 2006. The bhlh transcription factors, hes6 and mash1, are expressed in distinct subsets of
1001 cells within adult mouse taste buds. *Arch Histol Cytol,* 69**,** 189-98.
1002 **Shechtman, L. A., Piarowski, C. M., Scott, J. K., Golden, E. J., Gaillard, D. & Barlow, L.**
1003 **A.** 2021. Generation and culture of lingual organoids derived from adult mouse taste stem
1004 cells. *JoVE*, e62300.
1005 **Shechtman, L. A., Scott, J. K., Larson, E. D., Isner, T. J., Johnson, B. J., Gaillard, D.,**
1006 **Dempsey, P. J. & Barlow, L. A.** 2023. High sox2 expression predicts taste lineage
1007 competency of lingual progenitors in vitro. *Development,* 150.
1008 **Shingai, T. & Beidler, L. M.** 1985. Response characteristics of three taste nerves in mice. *Brain*
1009 *Res,* 335**,** 245-9.

1010 **Smith, J. C. 2001. The history of the "davis rig". *Appetite,* 36, 93-98.**
1011 **St. John, S. J. & Spector, A. C.** 1998. Behavioral discrimination between quinine and kcl is
1012 dependent on input from the seventh cranial nerve: Implications for the functional roles
1013 of the gustatory nerves in rats. *The Journal of Neuroscience,* 18**,** 4353.
1014 **Strell, C., Rodríguez-Tomàs, E. & Östman, A.** 2024. Functional and clinical roles of stromal
1015 pdgf receptors in tumor biology. *Cancer Metastasis Rev,* 43**,** 1593-1609.
1016 **Sukumaran, S. K., Lewandowski, B. C., Qin, Y., Kotha, R., Bachmanov, A. A. &**
1017 **Margolskee, R. F.** 2017. Whole transcriptome profiling of taste bud cells. *Scientific*
1018 *Reports,* 7**,** 7595.
1019 **Tizzano, M., Grigereit, L., Shultz, N., Clary, M. S. & Finger, T. E.** 2015.
1020 Immunohistochemical analysis of human vallate taste buds. *Chem Senses,* 40**,** 655-60.
1021 **Tomchik, S. M., Berg, S., Kim, J. W., Chaudhari, N. & Roper, S. D.** 2007. Breadth of tuning
1022 and taste coding in mammalian taste buds. *Journal of Neuroscience,* 27**,** 10840-10848.
1023 **Tomonari, H., Miura, H., Nakayama, A., Matsumura, E., Ooki, M., Ninomiya, Y. &**
1024 **Harada, S.** 2011. Gα-gustducin is extensively coexpressed with sweet and bitter taste
1025 receptors in both the soft palate and fungiform papillae but has a different functional
1026 significance. *Chemical Senses,* 37**,** 241-251.
1027 **Travers, J. B., Grill, H. J. & Norgren, R.** 1987. The effects of glossopharyngeal and chorda
1028 tympani nerve cuts on the ingestion and rejection of sapid stimuli: An electromyographic
1029 analysis in the rat. *Behavioural Brain Research,* 25**,** 233-246.
1030 **Van Elst, J. M., Ns, I. J., Mathijssen, R. H. J., Steeghs, N., Reyners, A. K. L. & De Haan, J.**
1031 **J.** 2022. Taste, smell and mouthfeel disturbances in patients with gastrointestinal stromal
1032 tumors treated with tyrosine-kinase inhibitors. *Support Care Cancer,* 30**,** 2307-2315.
1033 **Vigarios, E., Epstein, J. B. & Sibaud, V.** 2017. Oral mucosal changes induced by anticancer
1034 targeted therapies and immune checkpoint inhibitors. *Supportive Care in Cancer,* 25**,**
1035 1713-1739.
1036 **Wang, H., Iguchi, N., Rong, Q., Zhou, M., Ogunkorode, M., Inoue, M., Pribitkin, E. A.,**
1037 **Bachmanov, A. A., Margolskee, R. F. & Pfeifer, K.** 2009. Expression of the voltage-
1038 gated potassium channel kcnq1 in mammalian taste bud cells and the effect of its null-
1039 mutation on taste preferences. *Journal of Comparative Neurology,* 512**,** 384-398.
1040 **Wang, K., Mitoh, Y., Horie, K. & Yoshida, R.** 2025. Exploring the role of ccn3 in type iii cell
1041 of mice taste buds. *Journal of Neurochemistry,* 169**,** e16291.
1042 **Weaver, B. A.** 2014. How taxol/paclitaxel kills cancer cells. *Mol Biol Cell,* 25**,** 2677-81.
1043 **Yamada, Y., Takai, S., Watanabe, Y., Osaki, A., Kawabata, Y., Oike, A., Hirayama, A.,**
1044 **Iwata, S., Sanematsu, K., Tabata, S. & Shigemura, N.** 2021. Gene expression profiling
1045 of α-gustducin-expressing taste cells in mouse fungiform and circumvallate papillae.
1046 *Biochem Biophys Res Commun,* 557**,** 206-212.
1047 **Yang, H., Cong, W. N., Yoon, J. S. & Egan, J. M.** 2015. Vismodegib, an antagonist of
1048 hedgehog signaling, directly alters taste molecular signaling in taste buds. *Cancer Med,* 4**,**
1049 245-52.
1050 **Yang, R., Crowley, H. H., Rock, M. E. & Kinnamon, J. C.** 2000. Taste cells with synapses in
1051 rat circumvallate papillae display snap-25-like immunoreactivity. *J Comp Neurol,* 424**,**
1052 205-15.
1053 **Zaman, T., Vogt, D., Prokop, J., Alsabia, Q. A., Simms, G., Stafford, A., Luikart, B. W. &**
1054 **Williams, M. R.** 2024. Kit ligand and kit receptor tyrosine kinase sustain synaptic
1055 inhibition of purkinje cells. *eLife,* 12**,** RP89792.

1056 **Zhang, J., Jin, H., Zhang, W., Ding, C., O'keeffe, S., Ye, M. & Zuker, C. S.** 2019. Sour
1057 sensing from the tongue to the brain. *Cell,* 179**,** 392-402. e15.
1058

1059 **Figure Legends:**

1060 **Figure 1: TKIs selectively reduce expression of sweet type II TBC markers in organoids.**
1061 (**A**) Experimental design to test cabozantinib (Cabo), axitinib (Ax), and sunitinib (Sun) on TBC
1062 differentiation in organoids. (**B-E**) Compressed confocal z-stacks of control and TKI-treated
1063 organoids immunostained for markers of type II TBCs, PLCβ2 (**B**) and bitter/umami type II
1064 TBCs, GUST (**D**). Percentages of organoids containing 0, 1-9, or ≥ 10 cells immunopositive for
1065 PLCβ2 (**C**) or GUST (**E**) do not differ with treatment. Total organoids from 3 independent
1066 experiments: DMSO - 112; Cabo - 93; Ax - 110; Sun - 109. (**F-I**) Relative fold change in type II
1067 TBC marker expression via RT-qPCR. Each colored dot represents an individual sample of
1068 organoids pooled from 3 culture wells (over 200 organoids per sample). Within a condition,
1069 different shades represent 3 biological replicates and black dots are averages of each replicate.
1070 Ordinary one-way ANOVA with Dunnett's multiple comparisons test (**F-G**) or Holm-Sidak's
1071 multiple comparisons test (**I**) were used to compare average values (black line) for each marker
1072 across conditions (* $p \leq 0.05$, ** $p \leq 0.01$, *** $p \leq 0.001$).

1073

1074 **Figure 2: Cabozantinib changes the composition of type II TBC functional subtypes in**
1075 **CVP taste buds.** Mice were treated daily for 2 weeks (**A**) or 5 days per week for 4 weeks with
1076 drug or vehicle (**B**). (**C-N**) Quantification of the average number of stained cells per taste bud
1077 profile with corresponding representative images for SNAP25 immunofluorescence (IF) (**C-E**),
1078 PLCβ2-IF (**F-H**), *Tas1r2* HCR *in situ* hybridization (**I-K**) and GUST-IF (**L-N**). Representative
1079 images are compressed confocal z-stacks. Coarse dashed lines delineate basement membrane and
1080 apical epithelial surface; fine dashed lines encircle individual taste buds. Scale bar in E applies to
1081 H, K, and N. In all histograms, each dot represents the average taste cell tally from each mouse
1082 (N=3 per condition, ~80 taste buds/mouse). Unpaired t-test. Mean +/- SEM (* $p \leq 0.05$, **
1083 $p \leq 0.01$).

1084

1085

1086

1087

1088

1089 **Figure 3: Cabozantinib does not impact survival or induce transdifferentiation of sweet**
1090 **type II TBCs in CVP taste buds**. (**A**) *Kit*$^{CreER/+}$;*Rosa26*$^{YFP/YFP}$ mice were gavaged with
1091 tamoxifen daily for 5 days. Following a 3-day chase with daily cage changes, mice were gavaged
1092 with vehicle or cabozantinib 5 days per week for 14 days. (**B**) *Kit*-YFP^{+} cells per taste bud
1093 profile were unaltered by TKI treatment. (**C**) Compressed confocal z-stacks of *Kit*-YFP^{+} taste
1094 cells in CVP taste buds from vehicle- versus cabozantinib-treated mice. Coarse dashed lines
1095 delineate basement membrane and apical epithelial surface, fine dashed lines encircle individual
1096 taste buds. (**D-I**) The percentage of *Kit*-YFP^{+} cells (green in all panels) co-expressing PLCβ2 (**D-**
1097 **E, blue in E,** optical section), GUST (**F-G, Magenta in G**, optical section), or *Tas1r2* (**H-I,**
1098 **magenta in I,** compressed z-stack), is unchanged by drug treatment. Empty arrowheads in **E** and
1099 **I** indicate double-labeled cells. In all panels, values were calculated across >200 YFP^{+} cells and
1100 >200 taste buds per condition. Unpaired t-test performed for all quantifications. Mean+/-SEM.
1101
1102 **Figure 4: Cabozantinib shifts proportions of differentiating type II TBC subtypes in CVP**
1103 **taste buds**. (**A**) *Shh*$^{CreER/+}$;*Rosa26*$^{tdTomato/+}$ mice were treated with vehicle or cabozantinib 5 days
1104 per week for 14 days and dosed with tamoxifen on days 7 and 10 to label *Shh*$^{+}$ taste precursor
1105 cells. (**B**) The number of *Shh*-Tomato^{+} cells per taste bud profile was unaltered by cabozantinib.
1106 (**C**) Compressed confocal z-stacks of *Shh*-Tomato^{+} TBCs in taste buds from vehicle- versus
1107 cabozantinib-treated CVPs. Coarse dashed lines delineate basement membrane and apical
1108 epithelial surface, fine dashed lines encircle individual taste buds. (**D-I**) The percentage of *Shh*-
1109 Tomato^{+} cells (**magenta** in all panels) co-expressing PLCβ2 did not change (**D-E, green in E,**
1110 optical section). The percentage of Tomato^{+}/PLCβ2^{+} cells expressing GUST significantly
1111 increased, while the GUST^{-} percentage significantly decreased (**F-G, cyan in G,** optical section).
1112 The percentage of *Shh*-Tomato^{+} cells expressing *Tas1r2* was significantly decreased (**H-I, green**
1113 **in I,** compressed z-stacks). Empty arrowheads in **E**, **G** and **I** indicate double-labeled cells, white
1114 arrowheads in **E** and **G** indicate triple-labeled cells. In all panels, values were calculated across
1115 >400 Tomato^{+} cells and >200 taste buds per condition. Unpaired t-test (**B,D,H**) and two-way
1116 ANOVA with Sidak's multiple comparisons test (**F**) were performed to compare average values.
1117 Mean +/- SEM (* $p \leq 0.05$, ** $p \leq 0.01$).
1118

1119 **Figure 5: Sweet taste preference is diminished by cabozantinib.** (**A**) Mice treated with vehicle
1120 or cabozantinib 5 days per week for 4 weeks underwent behavioral assay training in week 3, and
1121 taste behavior testing in week four. (**B**) In a two-bottle taste test, only control mice preferred
1122 sweet solution at high SC45647 concentration (N= 9 control and 7 TKI mice). Preference score =
1123 volume of SC45647 consumed / total volume of water and SC45647 consumed. Dotted line at 50
1124 = no preference. (**C**) Brief access lickometer testing shows control mice prefer SC45647 at
1125 progressively higher concentrations while TKI-treated mice have no preference for SC45647
1126 over water (N= 9 control and 9 TKI mice). Lickometer responses for quinine (**D**) and citric acid
1127 (**E**) were unaltered by TKI treatment (N= 9 control and 9 TKI mice). Preference = average licks
1128 for tastant / average licks for water. All data were analyzed using Two-way ANOVA with
1129 Sidak's multiple comparisons test. Mean +/- SEM (** $p \leq 0.01$, *** $p \leq 0.001$, **** $p \leq 0.0001$).
1130

1131 **Figure 6: Conditional *Kit* knockout in the type II TBC lineage shifts type II TBC subtypes**
1132 **in CVP taste buds.** (**A**) *Kit* $^{fl/fl}$ (control) and *Pou2F3* $^{CreER/+}$*;Kit* $^{fl/fl}$ (experimental) mice were fed
1133 tamoxifen chow for 4 weeks. (**B-K**) Quantification of stained cells per taste bud profile with
1134 corresponding representative images for KIT-IF (**B-C**), SNAP25-IF (**D-E**), PLCβ2-IF (**F-G)**,
1135 *Tas1r2* HCR *in situ* hybridization (**H-I**) and GUSTDUCIN-IF (**J-K**). Representative images are
1136 compressed confocal z-stacks. Coarse dashed lines delineate basement membrane and apical
1137 epithelial surface, fine dashed lines encircle individual taste buds. Scale bar in **C** applies to **E**, **G**,
1138 **I** and **K**. In all histograms, each dot represents the average TBC tally from each mouse (N=4 per
1139 condition, ~80 taste buds/mouse). Unpaired t-test performed on all quantifications. Mean+/-SEM
1140 (**** $p \leq 0.0001$). (**L**) Proposed model of *Kit* function in type II TBC lineage, where *Pou2f3* $^{+}$
1141 precursor cells gives rise to all type II TBC subtypes, but those destined for a sweet cell fate
1142 upregulate *Kit*. Additionally, our pharmacological and genetic data support a model where KIT
1143 function is required for sweet type II cell fate in CVP. While different in details, we also
1144 conjecture a comparable model for FFP taste buds, but instead KIT function in *Pou2f3* $^{+}$ type II
1145 precursors is required for salt sensing type II cell fate (see **Figure S13**).
1146

Figures:

Figure 1:

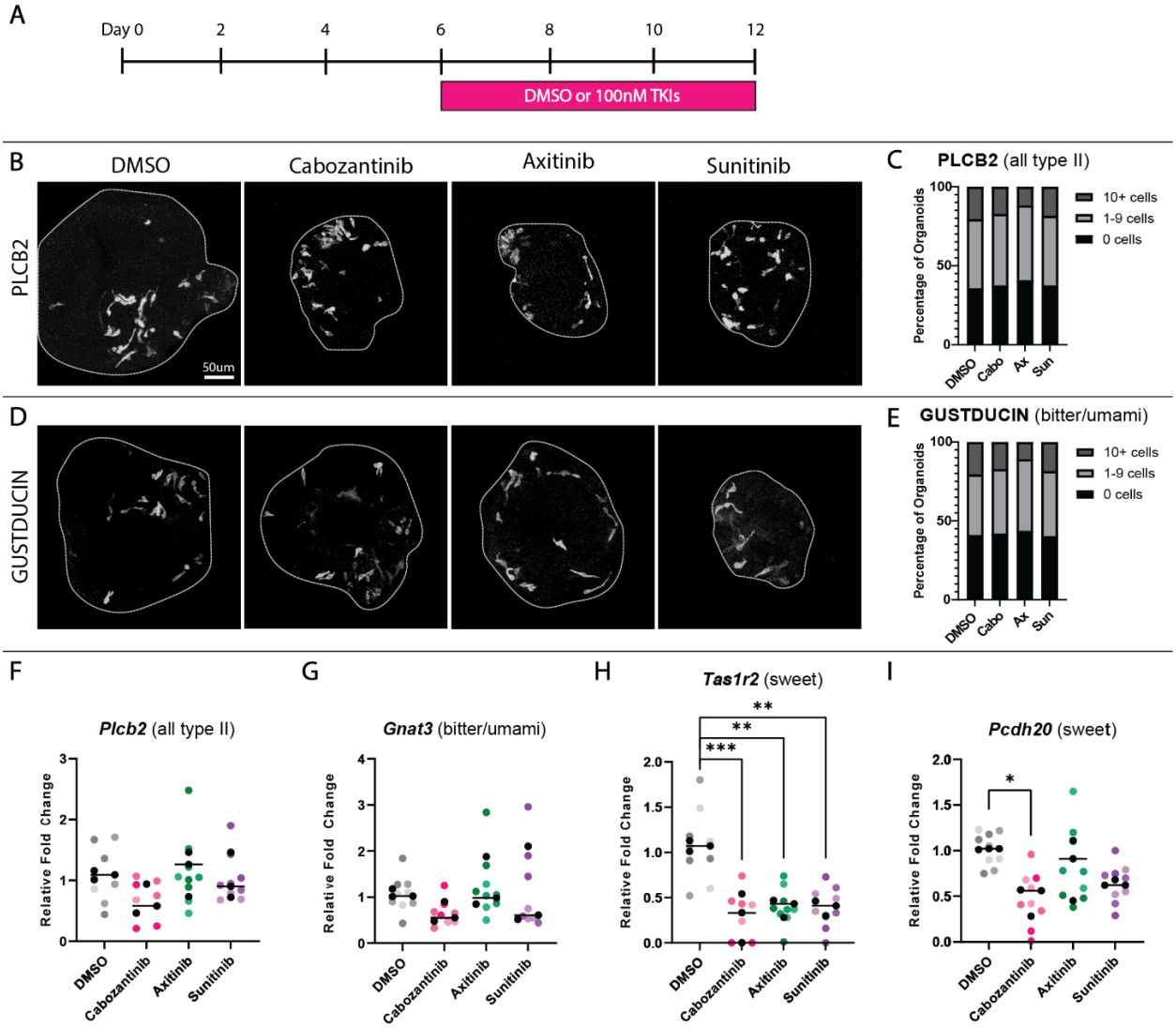

Figure 2:

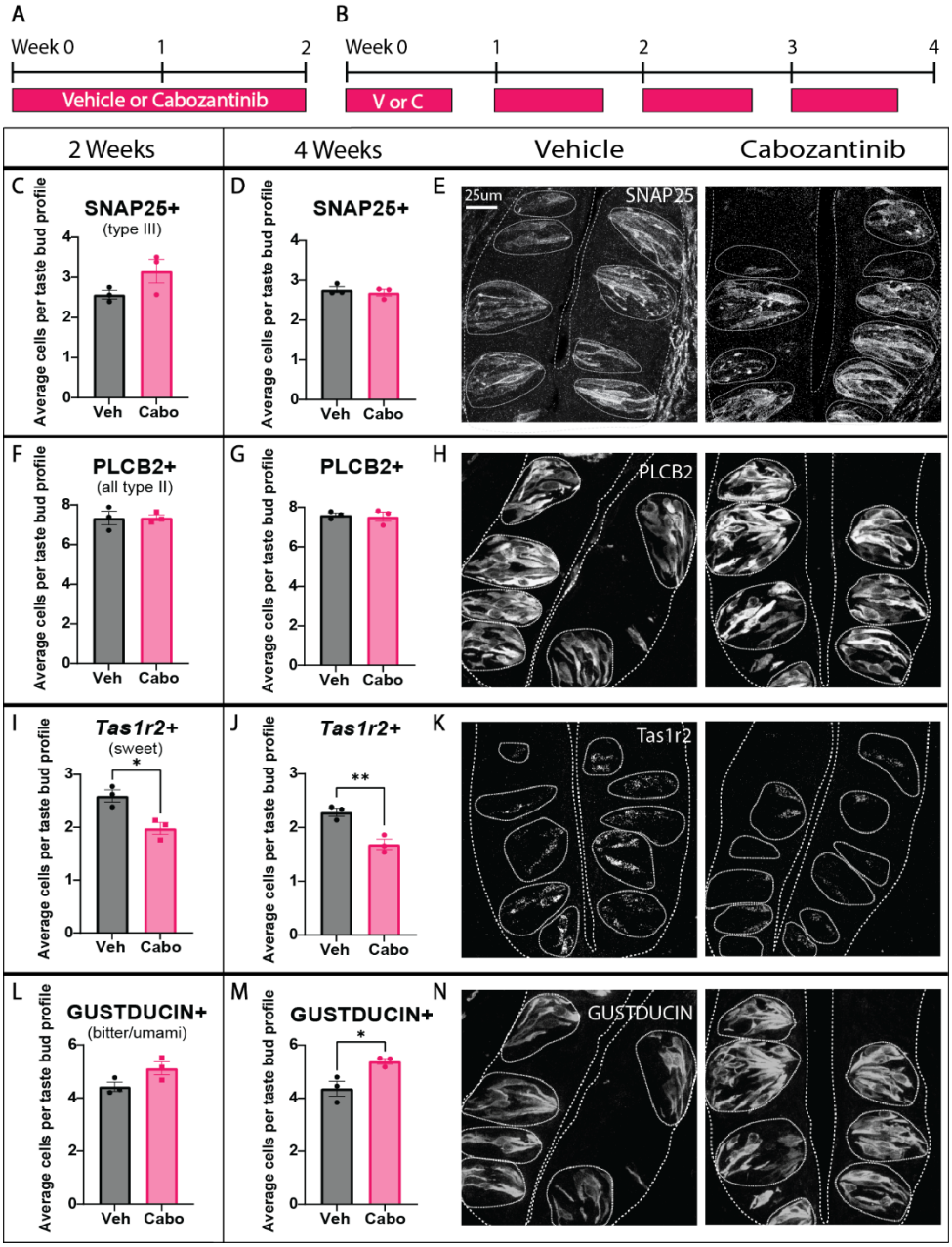
A
Week 0
1
2
Vehicle or Cabozantinib
B
Week 0
1
2
3
4
V or C
2 Weeks
4 Weeks
Vehicle
Cabozantinib
C
SNAP25+
(type III)
D
SNAP25+
E
25um
SNAP25
F
PLCB2+
(all type II)
G
PLCB2+
H
PLCB2
I
Tas1r2+
(sweet)
J
Tas1r2+
K
Tas1r2
L
GUSTDUCIN+
(bitter/umami)
M
GUSTDUCIN+
N
GUSTDUCIN
Average cells per taste bud profile
Veh
Cabo

Figure 3:

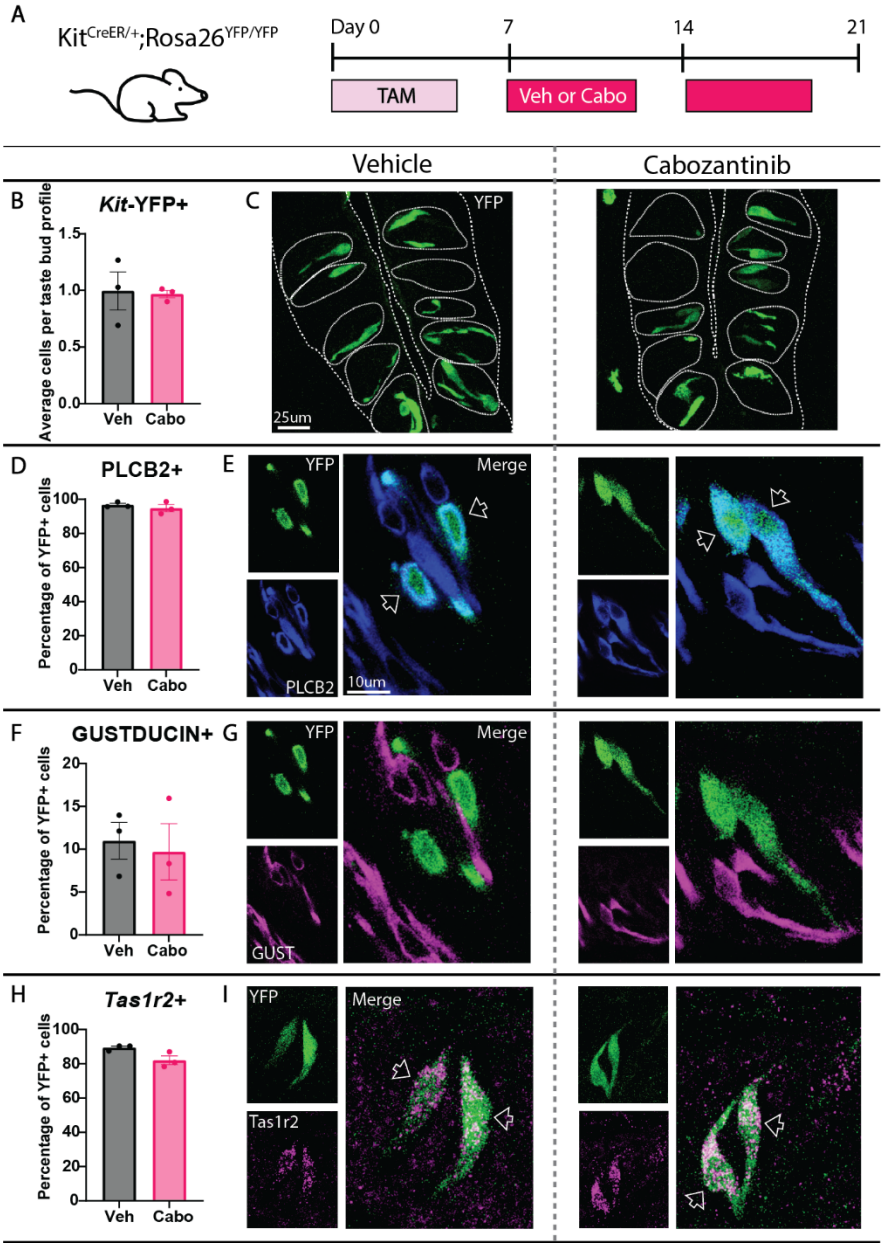
A
Kit^CreER/+;Rosa26^YFP/YFP
Day 0
7
14
21
TAM
Veh or Cabo
Vehicle
Cabozantinib
B
Kit-YFP+
Average cells per taste bud profile
1.5
1.0
0.5
0.0
Veh
Cabo
C
YFP
25um
D
PLCB2+
Percentage of YFP+ cells
100
80
60
40
20
0
Veh
Cabo
E
YFP
Merge
PLCB2
10um
F
GUSTDUCIN+
Percentage of YFP+ cells
20
15
10
5
0
Veh
Cabo
G
YFP
Merge
GUST
H
Tas1r2+
Percentage of YFP+ cells
100
80
60
40
20
0
Veh
Cabo
I
YFP
Merge
Tas1r2

Figure 4:

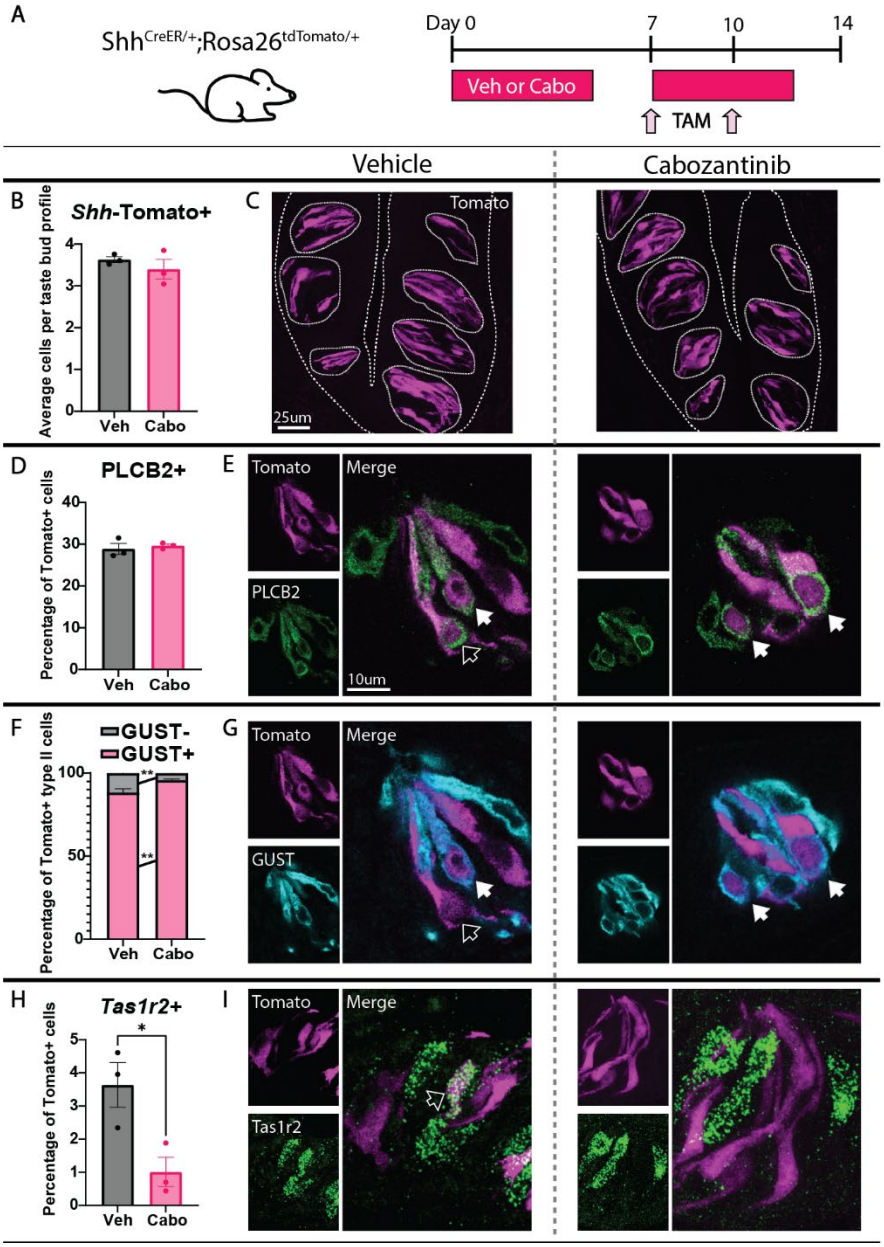
A
Shh^CreER/+;Rosa26^tdTomato/+
Day 0
7
10
14
Veh or Cabo
TAM
Vehicle
Cabozantinib
B
Shh-Tomato+
Average cells per taste bud profile
Veh
Cabo
C
Tomato
25um
D
PLCB2+
Percentage of Tomato+ cells
E
Tomato
Merge
PLCB2
10um
F
GUST-
GUST+
Percentage of Tomato+ type II cells
G
GUST
H
Tas1r2+
I
Tas1r2

Figure 5:

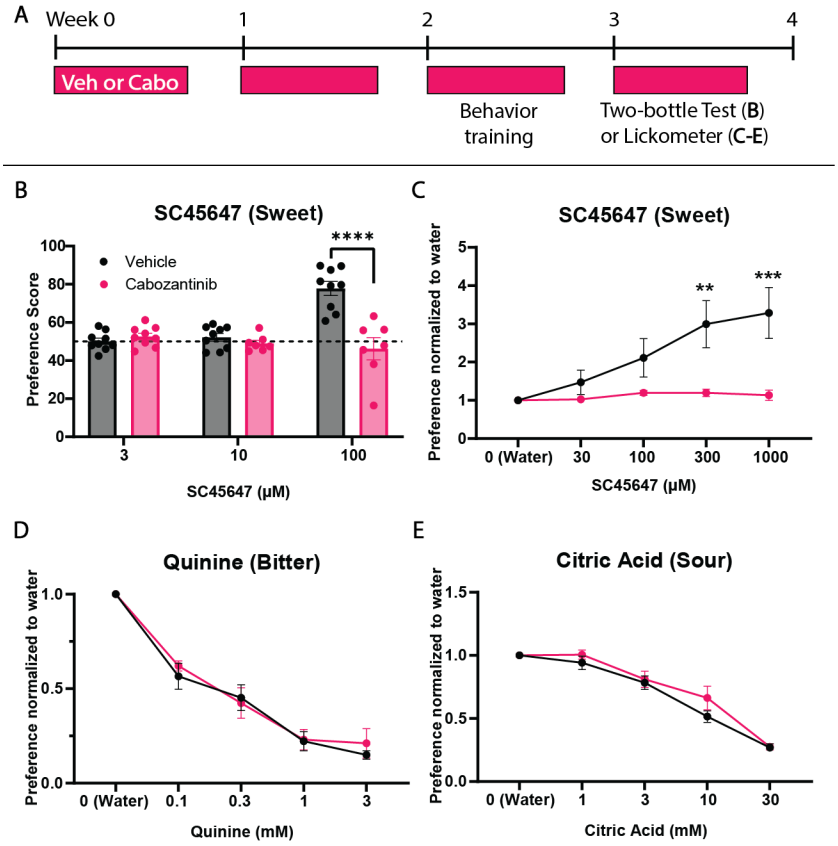
A
Week 0
1
2
3
4
Veh or Cabo
Behavior training
Two-bottle Test (B) or Lickometer (C-E)
B
SC45647 (Sweet)
Vehicle
Cabozantinib
Preference Score
****
SC45647 (μM)
C
SC45647 (Sweet)
Preference normalized to water
**
***
0 (Water)
SC45647 (μM)
D
Quinine (Bitter)
Preference normalized to water
Quinine (mM)
E
Citric Acid (Sour)
Preference normalized to water
Citric Acid (mM)

Figure 6:

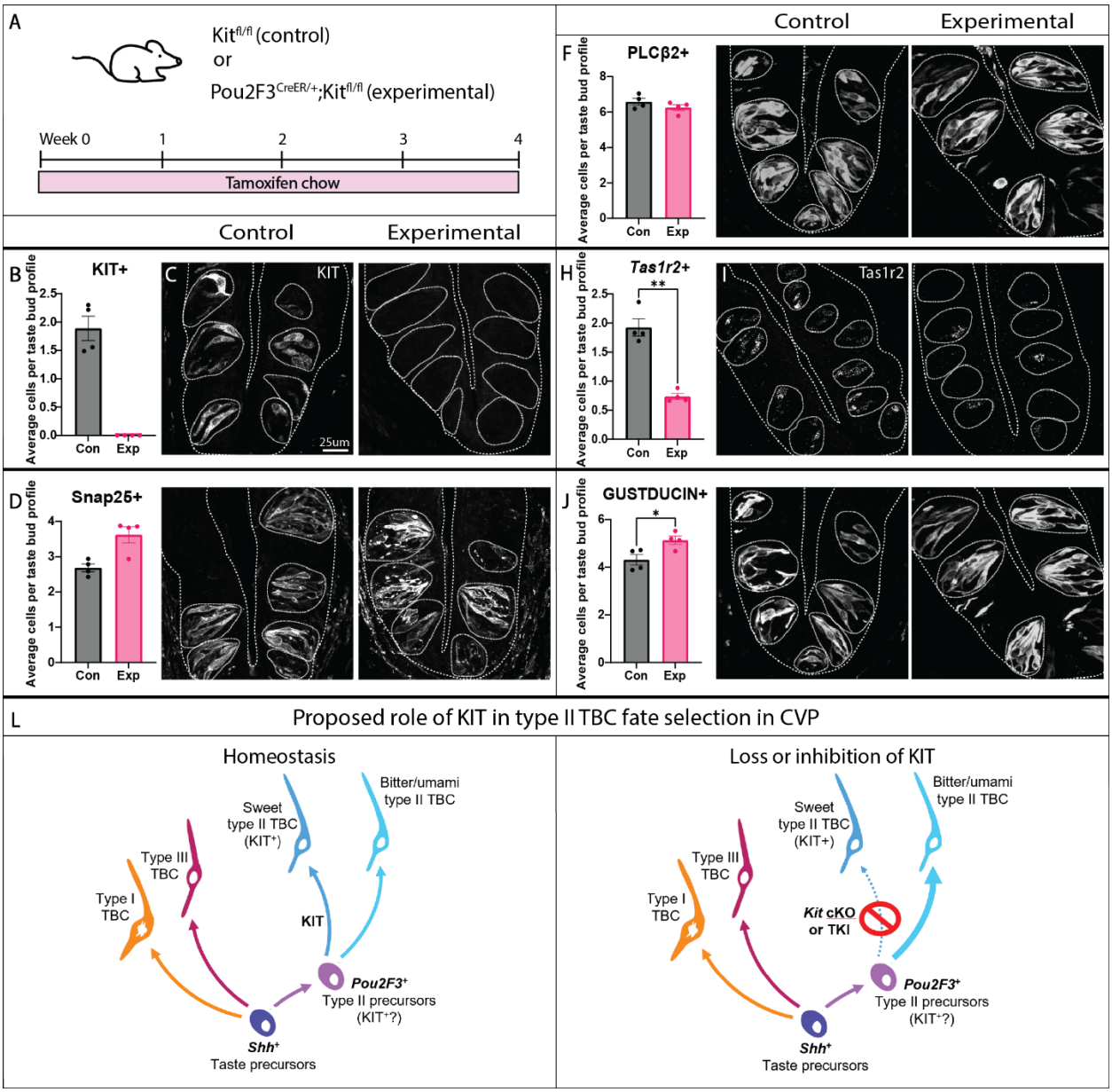
A
Kit fl/fl (control)
or
Pou2F3 CreER/+;Kit fl/fl (experimental)
Week 0
1
2
3
4
Tamoxifen chow
Control
Experimental
B
KIT+
Average cells per taste bud profile
Con
Exp
C
KIT
25um
D
Snap25+
F
PLCβ2+
H
Tas1r2+
**
I
Tas1r2
J
GUSTDUCIN+
*
L
Proposed role of KIT in type II TBC fate selection in CVP
Homeostasis
Sweet type II TBC (KIT+)
Bitter/umami type II TBC
Type III TBC
Type I TBC
KIT
Pou2F3+ Type II precursors (KIT+?)
Shh+ Taste precursors
Loss or inhibition of KIT
Kit cKO or TKI

Supplementary Material

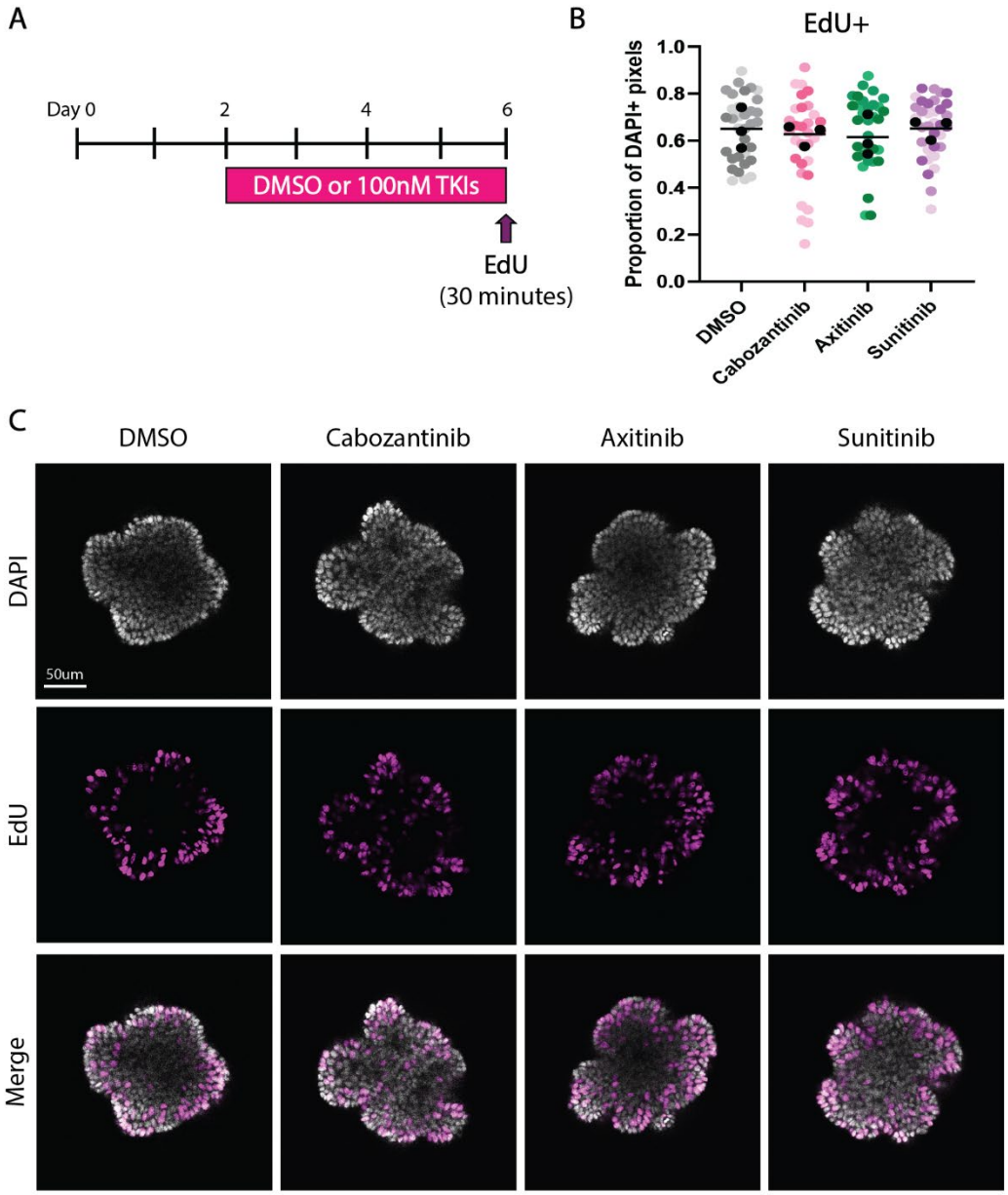

Figure S1. TKIs do not affect proliferation of taste progenitor cells in organoids. (**A**) Timeline of lingual organoid treatment with DMSO or 100 nM TKIs during the growth phase (day 2-6). EdU was added to the media for 30 minutes prior to harvest on day 6. (**B**) Drug treatment did not affect EdU labeling of organoids. Each colored dot represents the proportion of $DAPI^{+}$ pixels labeled with EdU in a single organoid. Within a treatment condition, different shades represent the 3 biological replicates, and black dots represent averages of each replicate. Ordinary one-way ANOVA with Dunnett's multiple comparisons test was used to compare the average values (black line) across conditions.

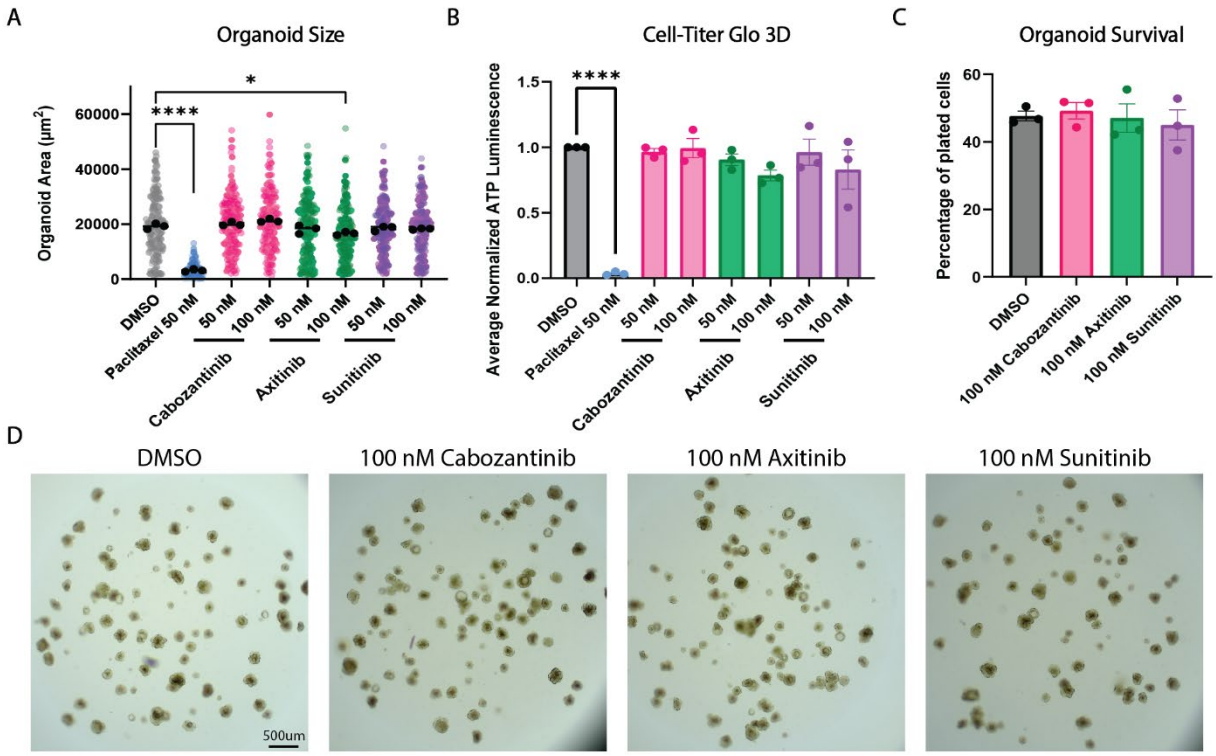

Figure S2: TKI treatment during the growth phase of culture does not affect growth or survival of lingual organoids. (**A**) Organoid area was not broadly affected by treatment with 50 or 100 nM TKIs (see Fig 1A) compared to negative control (DMSO), but was significantly reduced by paclitaxel (positive control). Each colored dot represents the area of one organoid. Within a treatment condition, different shades represent the 3 biological replicates, and black dots represent averages of each replicate. (**B**) Estimation of cell survival using Cell-Titer Glo® 3D was unaltered by TKI treatment compared to DMSO control, but was significantly diminished by paclitaxel. Each dot represents the average luminescence across 6 pooled wells for each of 3 biological replicates. (**C**) Organoid survival did not differ with condition. The number of organoids in each well at day 6 was divided by the number of plated cells at day 0 (200 cells per well). Each dot represents the average of three wells for each of 3 biological replicates. Ordinary one-way ANOVA with Dunnett's multiple comparisons test was performed on experimental averages in panel A and on all values in panels B and C. Mean +/- SEM (* $p \leq 0.05$, **** $p \leq 0.0001$). (**D**) Brightfield images of culture wells containing organoids treated with DMSO or 100 nM TKIs.

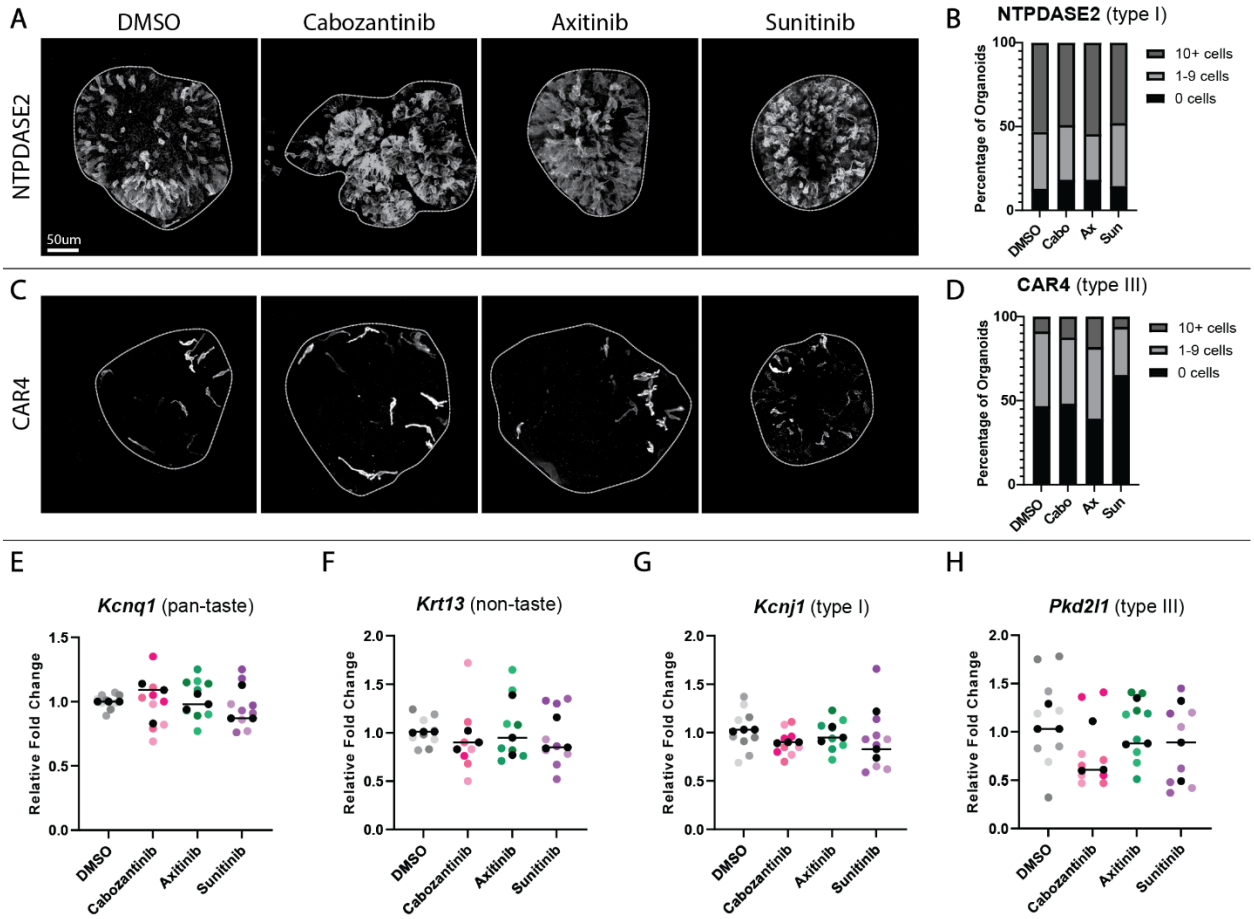

Figure S3: TKIs do not affect type I or type III TBCs or markers of taste vs non-taste epithelium. Compressed confocal z-stacks of control and TKI-treated organoids immunostained for markers of type I (NTPDase2) (**A**) and type III (CAR4) TBCs (**C**). Histograms showing percentages of organoids containing 0, 1-9, or ≥ 10 cells immunopositive for NTPDase2 (**B**) or CAR4 (**D**) reveal no change with drug treatment compared to controls. Total organoids obtained from 3 biological replicates: DMSO - 47; cabozantinib - 55; axitinib - 33; sunitinib - 48. Relative fold change in expression of pan-taste marker *Kcnq1* (**E**), non-taste marker *Krt13* (**F**), type I TBC marker *Kcnj1* (**G**) and type III TBC marker *Pkd2l1* (**H**) measured via RT-qPCR. Each colored dot represents an individual sample where organoids were pooled from three culture wells (~240 organoids per sample). Within a treatment condition, different shades represent the 3 biological replicates, and black dots represent averages of each replicate. Ordinary one-way ANOVA with Dunnett's multiple comparisons test was used to compare the average values (black line) for each marker across conditions.

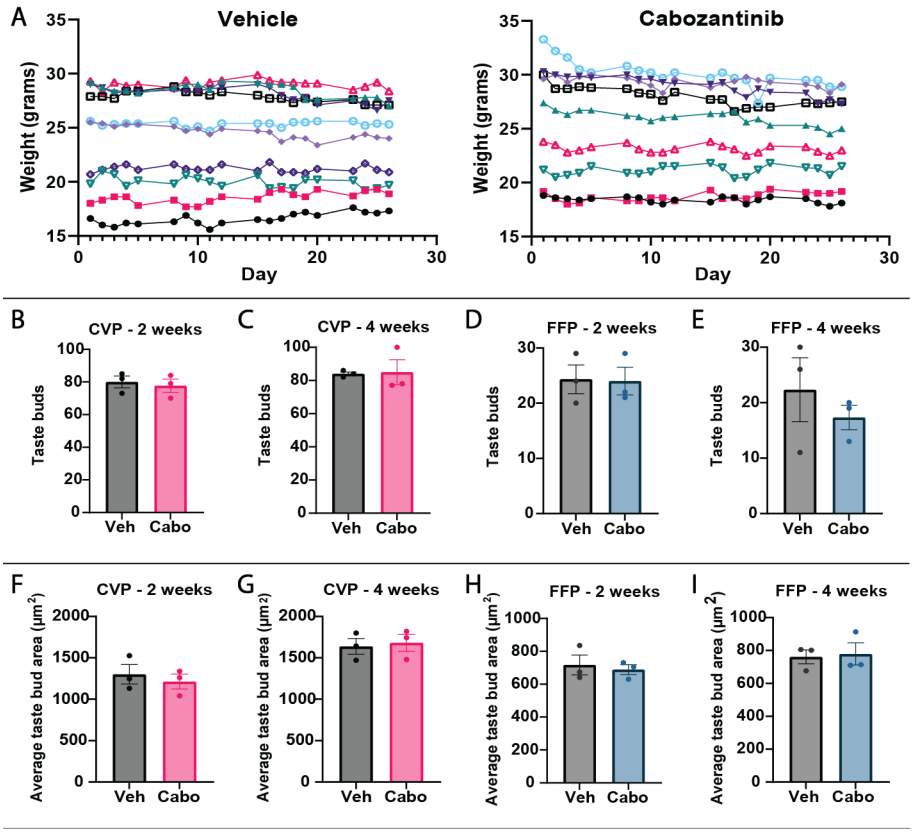

Figure S4: Cabozantinib does not affect mouse health or general taste bud homeostasis. (**A**) Weights of mice treated with vehicle or cabozantinib did not differ over 28 days. Weight was measured 5 days per week (symbols) and each colored line is an individual mouse (N=9 mice per condition). The number of CVP taste buds did not differ with treatment at 2 weeks (**B**) or 4 weeks (**C**). The number of FFP taste buds in the first 1.2 mm of the tongue was unaltered by cabozantinib treatment at 2 weeks (**D**) or 4 weeks (**E**). The average area of CVP (**F-G**) and FFP (**H- I**) taste bud profiles did not differ with treatment either at 2 weeks or 4 weeks (N=3 mice per condition). Unpaired t-test. Mean +/- SEM.

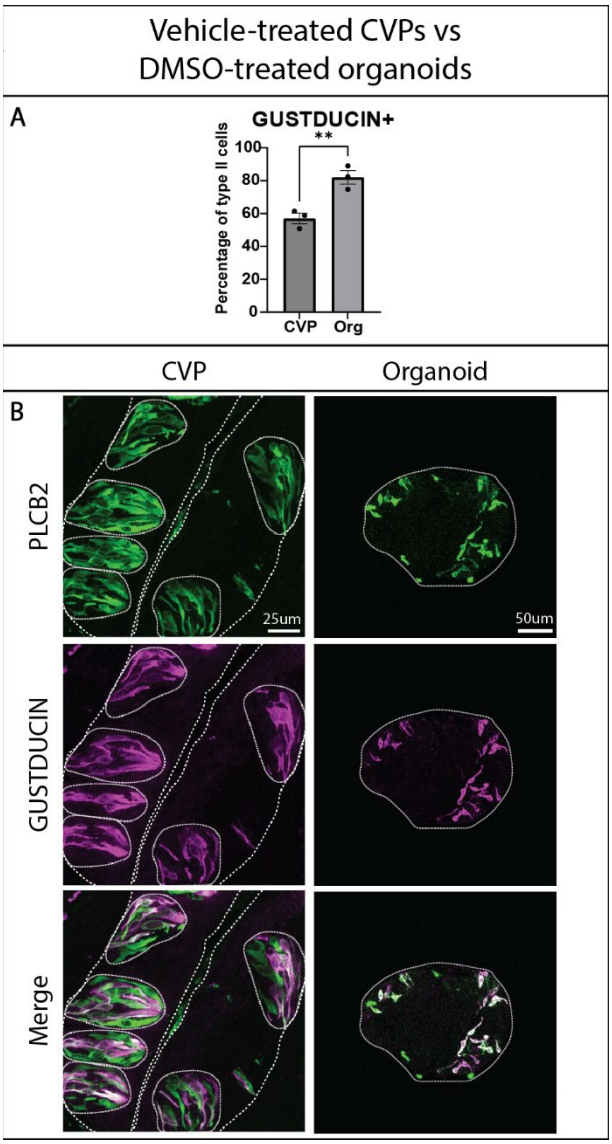

Figure S5: GUSTDUCIN$^+$ type II cells are over-represented in lingual organoids compared to CVP taste buds. (A) The percentage of PLCβ2$^+$ type II cells expressing GUST is higher in organoids compared to *in vivo*. CVP values are from vehicle-treated mice after 4 weeks of treatment (see Figure 2), while organoid values are from organoids treated with DMSO during the differentiation phase (see **Figure 1**). Each dot in the organoid condition is the average percentage across ~10 organoids for each biological replicate. (**B**) Compressed confocal z-stacks showing vehicle-treated CVP trenches compared to DMSO-treated organoids immunostained for PLCβ2 (green) and GUST (magenta). In the CVP, coarse dashed lines delineate basement membrane and apical surface of epithelium, fine dashed lines encircle individual taste buds. Unpaired t-test. Mean +/- SEM (** $p \leq 0.01$).

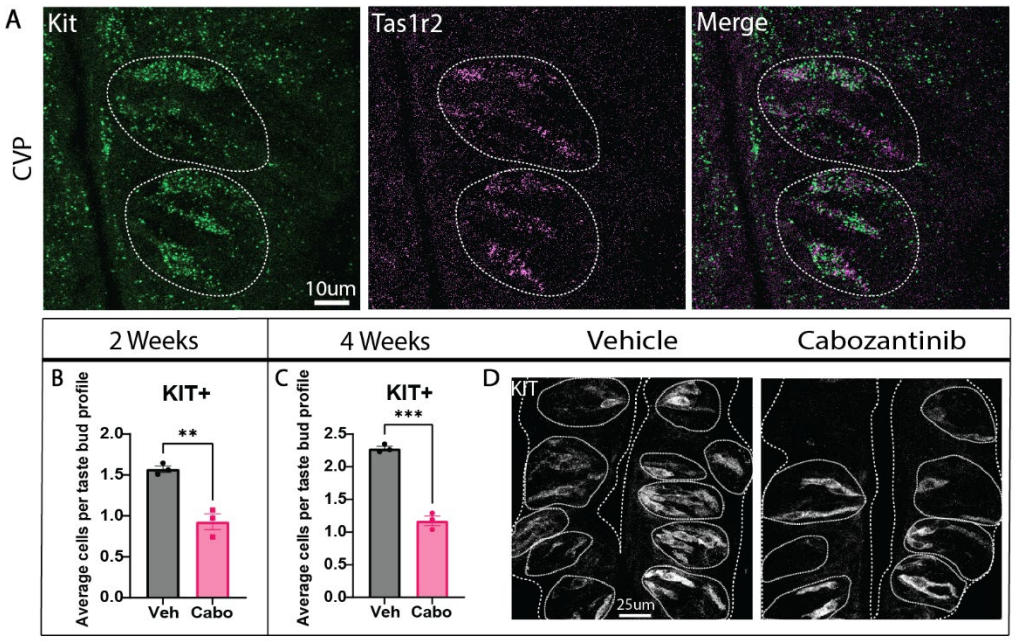

Figure S6: *Kit* marks *Tas1r2*$^{+}$ sweet cells in the CVP. (**A**) In the CVP, HCR *in-situ* hybridization using probes against *Kit* and *Tas1r2* reveals extensive co-expression in taste cells. Dashed lines circle individual taste buds. KIT-IF taste cells per taste bud profile are reduced in the CVP of mice treated with cabozantinib compared to controls at 2 weeks (**B**) and 4 weeks (**C**). (**D**) Compressed confocal z-stacks of KIT immunostaining in mice treated with vehicle or cabozantinib after 4 weeks. Coarse dashed lines delineate basement membrane and apical surface of epithelium, fine dashed lines encircle individual taste buds (N=3 mice per condition). Unpaired t-test. Mean+/-SEM (** $p \leq 0.01$, **** $p \leq 0.0001$).

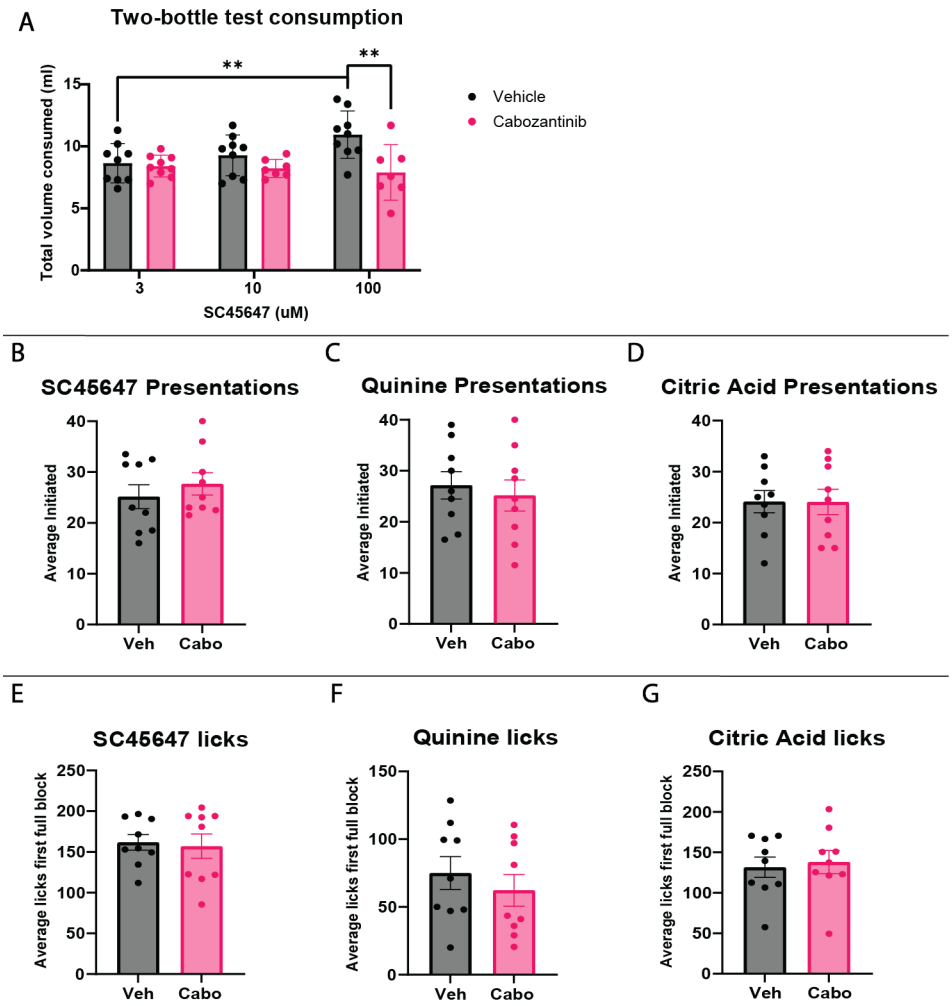

Figure S7: Cabozantinib does not change participation effort or thirst of mice in taste behavior assays. (**A**) Total consumption of liquid across 48 hrs of testing at each tastant concentration did not differ between control and TKI-treated mice, except at the highest concentration of SC45647 where control mice drank significantly more than drug treated mice. (**B-D**) Average presentations initiated across 2 days of lickometer testing for SC45647 (**B**), quinine (**C**), and citric acid (**D**) did not differ with treatment. The maximum number of presentations per testing session was 40. (**E-G**) Average number of licks during the first full testing block (one presentation of each concentration) across 2 testing days did not differ for SC45647 (**E**), quinine (**F**), and citric acid (**G**). Two-way ANOVA with both Sidak's and Tukey's multiple comparisons tests performed on data in panel A (N = control 9 and 7 TKI mice). Unpaired t-tests performed on panels B-G (N=9 mice per condition). Mean+/-SEM (** $p \leq 0.01$).

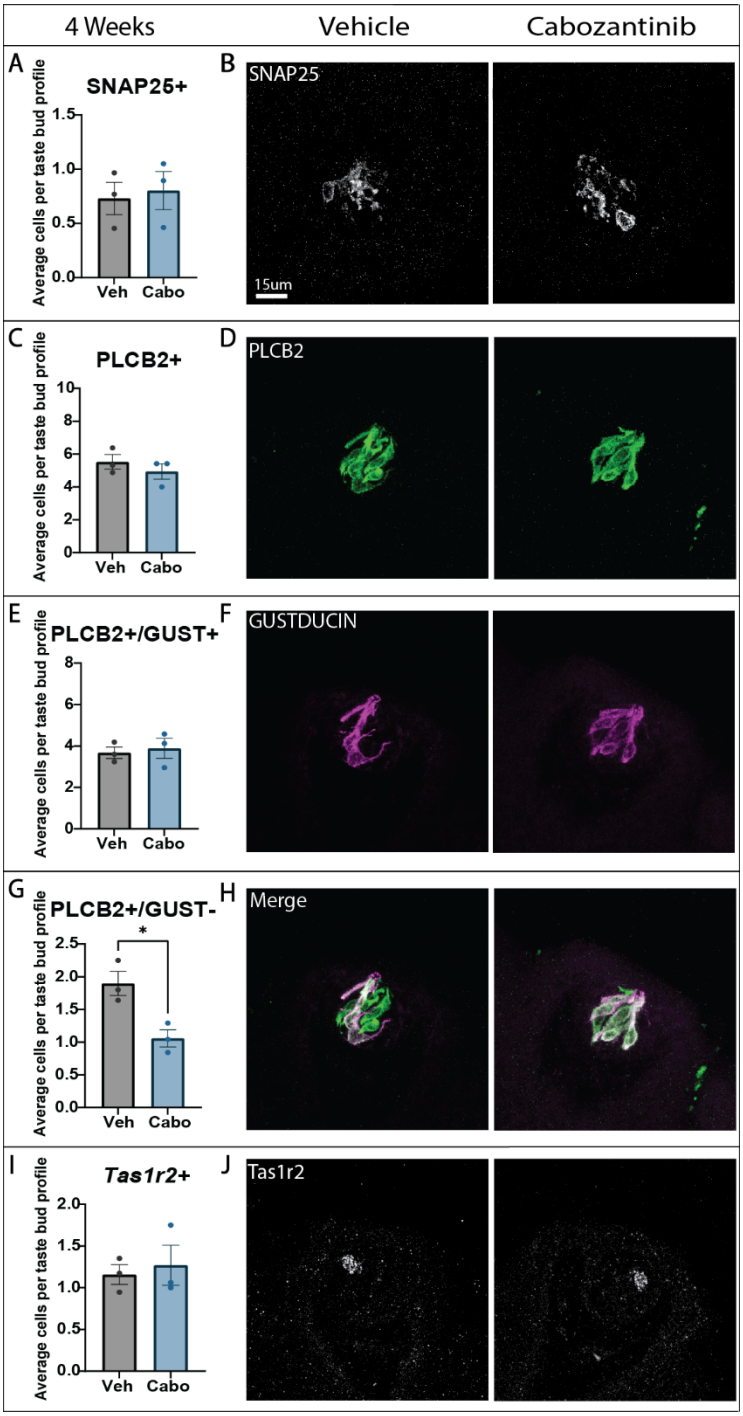

Figure S8: Cabozantinib changes the composition of PLCβ2+ type II subtypes in FFP taste buds. Quantification of the average number of taste cells per taste bud profile with corresponding representative images for SNAP25-IF (**A-B**), PLCβ2-IF (**C-D**), PLCβ2^{+}/GUST^{+} IF (**E-F**), PLCβ2^{+}/GUST^{-} IF (**G-H**) and *Tas1r2* HCR *in situ* hybridization (**I-J**). Representative images are compressed confocal z-stack projections. Scale bar in B applies to D, F, H and J. In all histograms, each dot represents the average taste cell tally from one mouse (N=3 per condition, ~10-30 taste buds/mouse). Unpaired t-test. Mean+/-SEM (* $p \leq 0.05$).

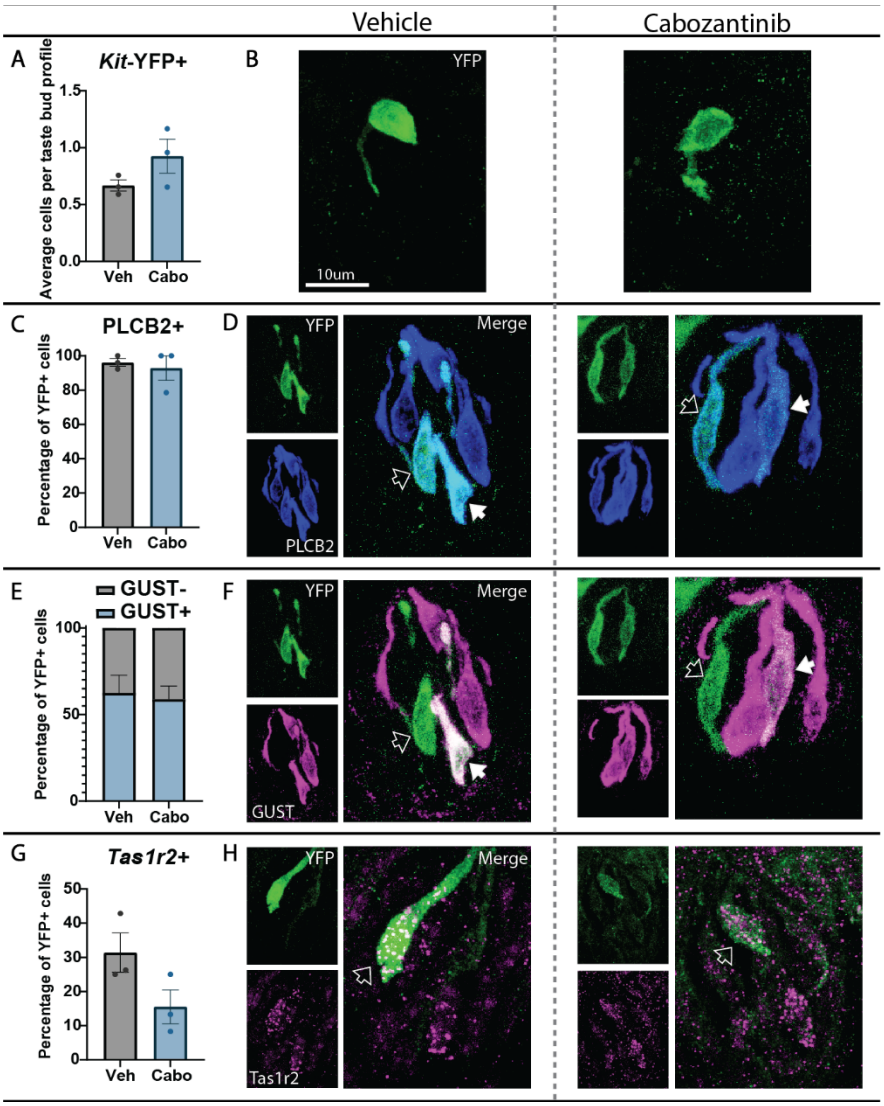

Figure S9: Cabozantinib does not induce cell death or transdifferentiation of *Kit*$^{+}$ cells in FFP taste buds. (**A**) In *Kit*$^{CreER/+}$;*Rosa26*$^{YFP/YFP}$ mice, the average number of *Kit*-YFP^{+} cells per taste bud profile is unaltered by TKI treatment. (**B**) Compressed confocal z-stacks of *Kit*-YFP^{+} taste cells in FFP taste buds from vehicle- vs cabozantinib-treated mice. (**C, E, G**) The percentage of *Kit*-YFP^{+} cells (green in all panels) co-expressing PLCβ2 (**C-D, blue in D**), GUST (**E-F, Magenta in F**) or *Tas1r2* (**G-H, magenta in H**) is unchanged by drug treatment (compressed confocal z-stacks in all panels). Empty arrowheads in **D**, **F** and **H** indicate double-labeled cells, white arrowheads in **D** and **F** indicate triple-labeled cells. In all panels, values were calculated across >50 YFP^{+} cells and >30 taste buds per condition. Unpaired t-test performed for all quantifications. Mean+/-SEM.

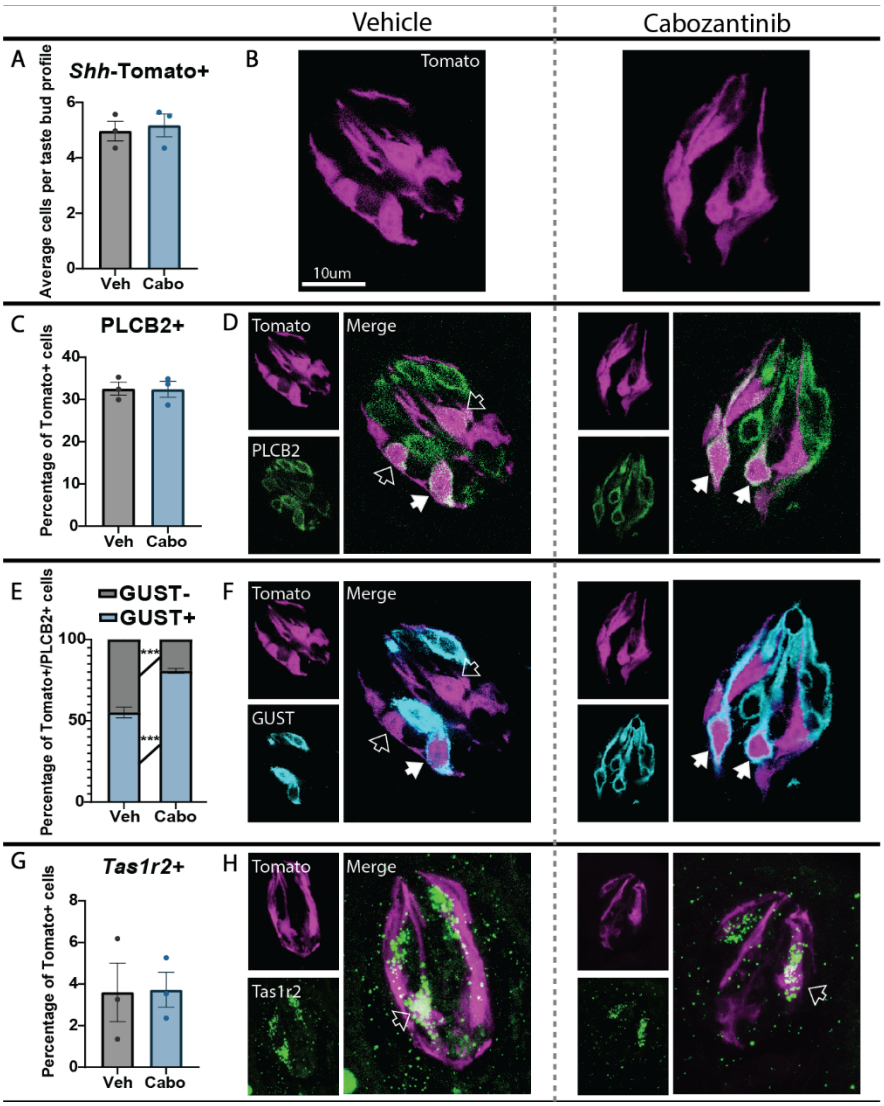

Figure S10: Cabozantinib increases differentiation of PLCß2^{+}/GUST^{+} cells in FFP taste buds. (**A**) In *Shh*$^{CreER/+}$;*Rosa26*$^{tdTomato/+}$ mice, the average number of *Shh*-Tomato^{+} cells per taste bud profile was unaltered by cabozantinib treatment. (**B**) Optical section of *Shh*-tomato^{+} taste cells in FFP taste buds from vehicle- vs cabozantinib-treated mice. (**C, E, G**) The percentage of *Shh*-Tomato^{+} cells (**magenta** in all panels) co-expressing PLCβ2 did not change (**C-D, green in D,** optical section). The percentage of *Shh*-Tomato^{+} cells expressing GUST significantly increased and the percentage not expressing GUST significantly decreased (**E-F, cyan in F,** optical section), while the percentage of *Shh*-Tomato^{+} expressing *Tas1r2* did not change (**H-I, green in I,** compressed z-stacks). Empty arrowheads in **D**, **F** and **H** indicate double-labeled cells, white arrowheads in **D** and **F** indicate triple-labeled cells. In all panels, values were calculated across >550 Tomato^{+} cells and >95 taste buds per condition. Unpaired t-test performed for panels **A**, **C** and **G**. Two-way ANOVA with Sidak's multiple comparisons test performed for panel **E**. Mean+/-SEM (*** $p \leq 0.001$).

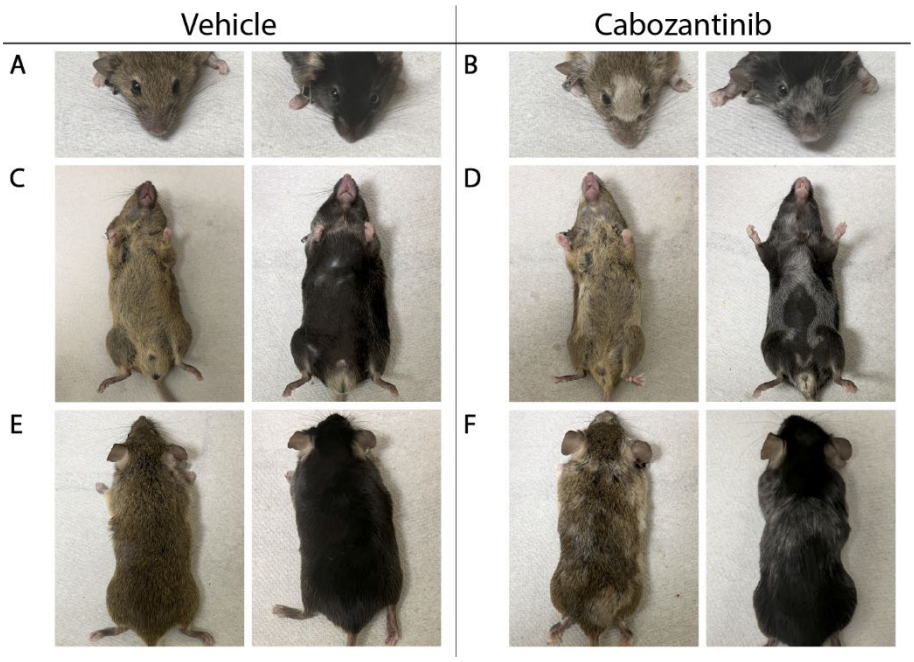

Figure S11: Cabozantinib treatment causes fur depigmentation. Cabozantinib causes depigmentation of facial (**A-B**), stomach (**C-D**) and back (**E-F**) fur. Depigmentation was evident in mice of mixed background with brown or black fur.

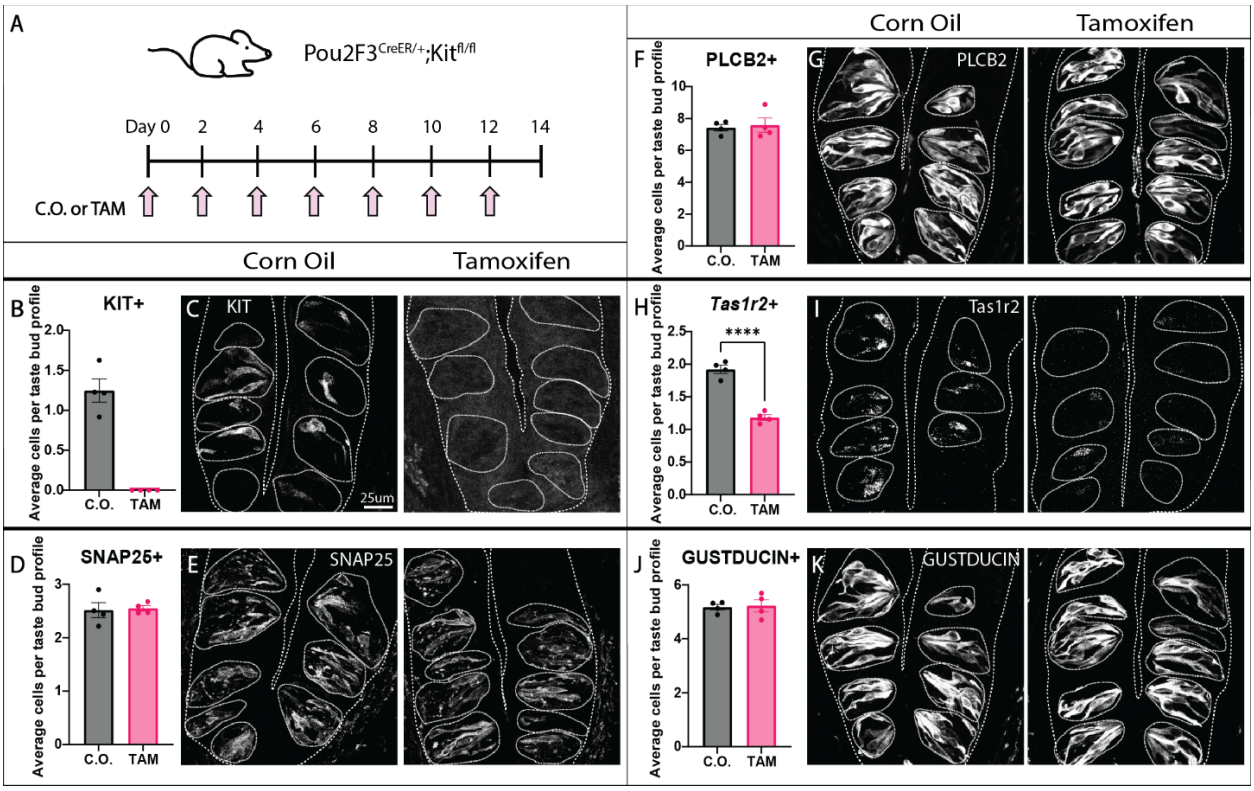

Figure S12: Two-week Kit knockout reduces sweet cells but does not affect bitter/umami cells in CVP. (**A**) *Pou2F3$^{CreER/+}$;Kit$^{fl/fl}$* mice were gavaged with corn oil or tamoxifen every other day for 14 days. (**B-K**) Quantification of stained cells per taste bud profile with corresponding representative images for KIT-IF (**B-C**), SNAP25-IF (**D-E**), PLCβ2-IF (**F-G)**, *Tas1r2* HCR *in situ* hybridization (**H-I**) and GUST-IF (**J-K**). Representative images are compressed confocal z-stacks. Coarse dashed lines delineate basement membrane and apical epithelial surface, fine dashed lines encircle individual taste buds. Scale bar in **C** applies to **E**, **G**, **I** and **K**. In all histograms, each dot represents the average TBC tally from each mouse (N=4 per condition, ~80 taste buds/mouse). Unpaired t-test performed on all quantifications. Mean+/-SEM (**** $p \leq 0.0001$).

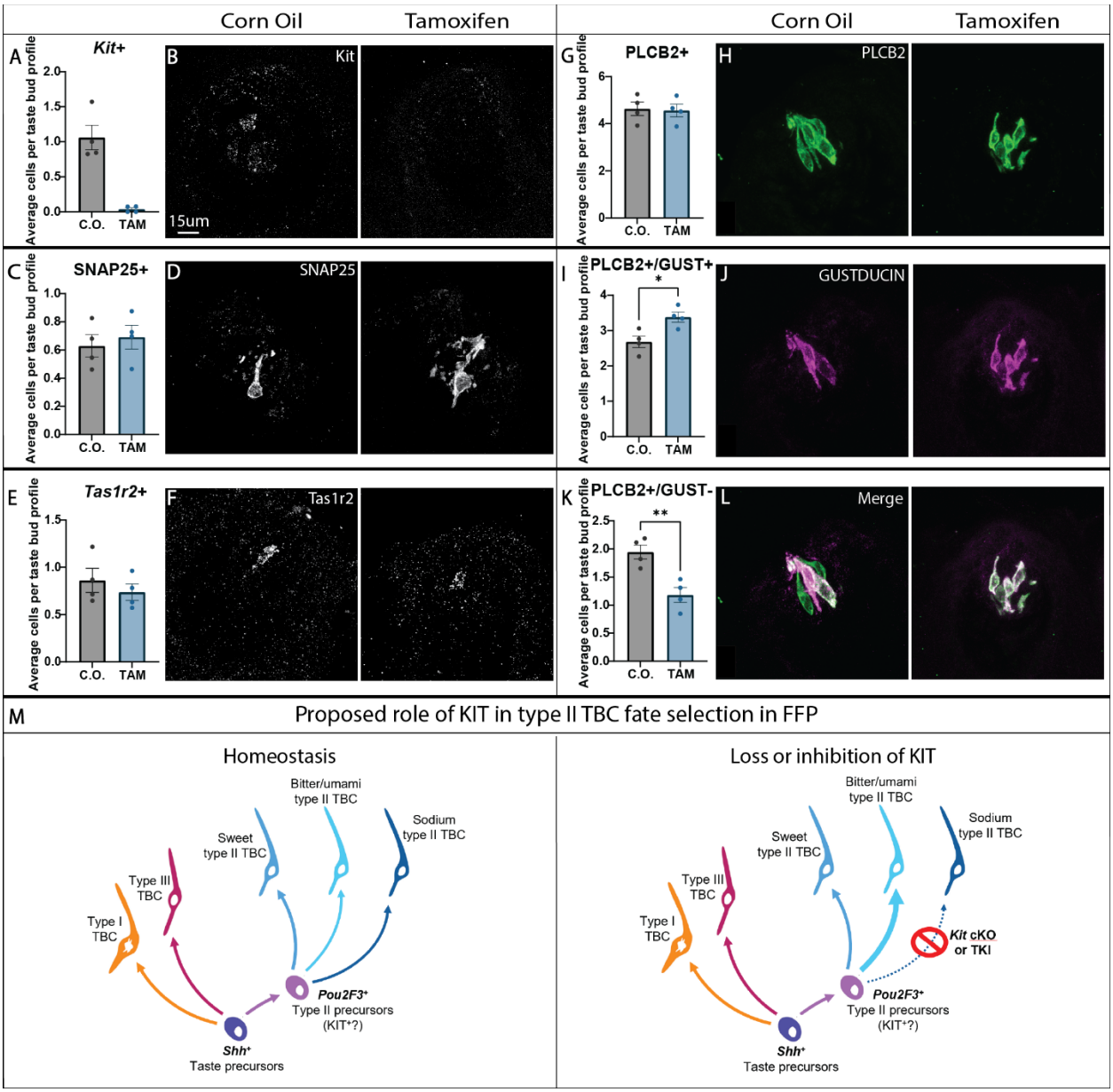

Figure S13: *Kit* knockout causes a fate switch in PLCβ2+ cells in FFP taste buds. (**A-L**) Quantification of the average number of stained cells per taste bud profile with corresponding representative images for *Kit* HCR *in situ* hybridization (**A-B**), SNAP25 IF (**C-D**), *Tas1r2* HCR *in situ* hybridization (**E-F**), PLCβ2 IF (**G-H**), PLCβ2^{+}/GUST^{+} IF (**I-J**), and PLCβ2^{+}/GUST^{-} IF (**K-L**). Representative images are compressed confocal z-stack projections. Scale bar in B applies to D, F, H, J and L. In all histograms, each dot represents the average taste cell tally from one mouse (N=4 per condition, ~15 taste buds/mouse). Mann-Whitney test performed on data from panel A, unpaired t-test performed on data from panels C, E, G, I, K and M. Mean +/- SEM (* $p \leq 0.05$, ** $p \leq 0.01$). (**M**) Proposed model of *Kit* function in type II TBC lineage. We propose that a *Pou2f3*$^{+}$ precursor population gives rise to all type II TBC subtypes. Our pharmacological and genetic data support a model where KIT function is required for sodium-sensing type II cell fate in FFP.

Table S1: RT-qPCR Primers

Gene name	Refseq	Forward Sequence (5’ --> 3’)	Reverse Sequence (5’ --> 3’)
Rpl19	NM_009078.2	GGTCTGGTTGGATCCCAATG	CCCGGGAATGGACAGTCA
Kcnq1	NM_008434.2	TTTGTTCATCCCCATCTCAG	GTTGCTGGGTAGGAAGAG
Krt13	NM_010662.2	TCATCTCGGTTTGTCACTGGA	TGATCTTCTCGTTGCCAGAGAG
Kcnj1	NM_001168354.1	GACAGCTGAATGGGTGAGGT	ATCAGATGCCCTGAAACTGG
Pkd2l1	NM_181422	TACAGCGACCCTCCTTCCC	CCTCTGATGCTCCGACAGATATG
Plcb2	NM_177568.2	GAGCAAATCGCCAAGATGAT	CCTTGTCTGTGGTGACCTTG
Gnat3	NM_001081143.1	ATCCAGGAATCCAAGCCTGC	TGGTTTTCACCCGGGAATGT
Tas1r2	NM_031873.1	TGGCAGCTACTCAGGGAGAT	GAGTAGGAGGCGATGCTTTG
Pcdh20	NM_178685	GGGGCAAGCATCAAAACACATT	AAACACCAAGCAAGCAAGTAGAGATT

Table S2: Primary Antibodies

Primary Antibody	**Source**	**Dilution**
Rat anti KRT8	DHSB; Troma-IS	1:250
Rabbit anti NTPDASE2	CHUQ; mN2-36LI6	1:300
Guinea Pig anti PLCβ2 (tissue)	Phosphosolutions; Purple antiserum Bleed: 8/24/21 RRID: AB_3097715	1:500
Guinea Pig anti PLCβ2 (organoids)	Phosphosolutions; Blue affinity purified Bleed: 8/24/21 RRID: AB_2934326	1:250
Goat anti GUSTDUCIN	Aviva Systems Biology; OAEB00418	1:1,000 (tissue), 1:500 (organoids)
Goat anti SNAP25	GeneTex; GTX89577	1:200
Goat anti CAR4	R&D Systems; AF2414	1:50
Rabbit anti KIT	Cell Signaling Technology; 3074	1:200
Chicken anti GFP	Aves Labs; GFP 1020	1:500